



US006108576A

United States Patent [19]

[11] **Patent Number:** **6,108,576**

Alfano et al.

[45] **Date of Patent:** ***Aug. 22, 2000**

[54] **TIME-RESOLVED DIFFUSION TOMOGRAPHIC 2D AND 3D IMAGING IN HIGHLY SCATTERING TURBID MEDIA**

5,528,365	6/1996	Gonatas	356/340
5,529,065	6/1996	Tsuchiya	128/633
5,555,885	9/1996	Chance	128/654
5,596,987	1/1997	Chance	128/633
5,606,969	3/1997	Butler et al.	128/653.1
5,625,458	4/1997	Alfano et al.	356/446
5,630,423	5/1997	Wang et al.	128/664
5,644,429	7/1997	Alfano et al.	359/559
5,664,574	9/1997	Chance	128/664

[75] Inventors: **Robert R. Alfano; Wei Cai**, both of Bronx, N.Y.; **Swapan K. Gayen**, Marlboro, N.J.

[73] Assignee: **The Research Foundation of City College of New York**, New York, N.Y.

[*] Notice: This patent is subject to a terminal disclaimer.

[21] Appl. No.: **08/797,163**

[22] Filed: **Feb. 10, 1997**

Related U.S. Application Data

[63] Continuation-in-part of application No. 08/797,028, Feb. 7, 1997, which is a continuation-in-part of application No. 08/618,471, Mar. 18, 1996.

[51] **Int. Cl.**⁷ **A61B 6/00**

[52] **U.S. Cl.** **600/476; 600/473; 600/310**

[58] **Field of Search** 128/633, 665, 128/664; 356/318, 446; 600/310, 473, 476, 475

[56] **References Cited**

U.S. PATENT DOCUMENTS

4,597,392	7/1986	Opitz et al.	128/637
4,612,938	9/1986	Dietrich et al.	128/665
4,945,239	7/1990	Wist et al.	250/358.1
5,203,339	4/1993	Knuttel et al.	128/665
5,303,026	4/1994	Strobl et al.	356/318
5,303,710	4/1994	Bashkansky et al.	128/665
5,333,610	8/1994	Hirao	128/633
5,349,951	9/1994	Ito et al.	128/633
5,353,799	10/1994	Chance	128/664
5,371,368	12/1994	Alfano et al.	250/341.1
5,413,098	5/1995	Benaron	128/633
5,416,582	5/1995	Knutson et al.	356/349
5,441,054	8/1995	Tsuchiya	128/665
5,517,987	5/1996	Tsuchiya	128/633

Primary Examiner—Marvin M. Lateef
Assistant Examiner—Shawna J. Shaw
Attorney, Agent, or Firm—Kriegsman & Kriegsman

[57] **ABSTRACT**

A method for imaging objects in highly scattering turbid media. According to one embodiment of the invention, the method involves using a plurality of intersecting source/detectors sets and time-resolving equipment to generate a plurality of time-resolved intensity curves for the diffusive component of light emergent from the medium. For each of the curves, the intensities at a plurality of times are then inputted into the following inverse reconstruction algorithm to form an image of the medium:

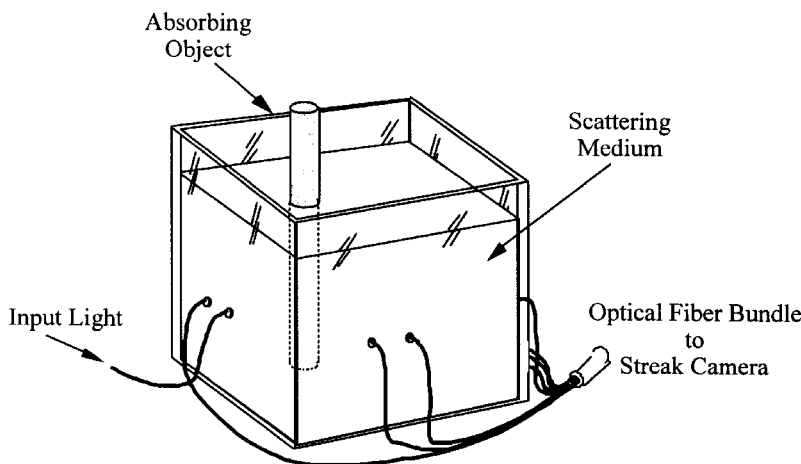
$$X^{(k+1)T} = [Y^T W + X^{(k)T} \Lambda] [W^T W + \Lambda]^{-1}$$

wherein W is a matrix relating output at source and detector positions r_s and r_d , at time t, to position r, Λ is a regularization matrix, chosen for convenience to be diagonal, but selected in a way related to the ratio of the noise, $\langle nn \rangle$ to fluctuations in the absorption (or diffusion) X_j that we are trying to determine:

$$\Lambda_{ij} = \lambda_j \delta_{ij} \text{ with } \lambda_j = \langle nn \rangle / \langle \Delta X_j \Delta X_j \rangle$$

Y is the data collected at the detectors, and X^k is the kth iterate toward the desired absorption information. An algorithm, which combines a two dimensional (2D) matrix inversion with a one-dimensional (1D) Fourier transform inversion is used to obtain images of three dimensional hidden objects in turbid scattering media.

51 Claims, 13 Drawing Sheets



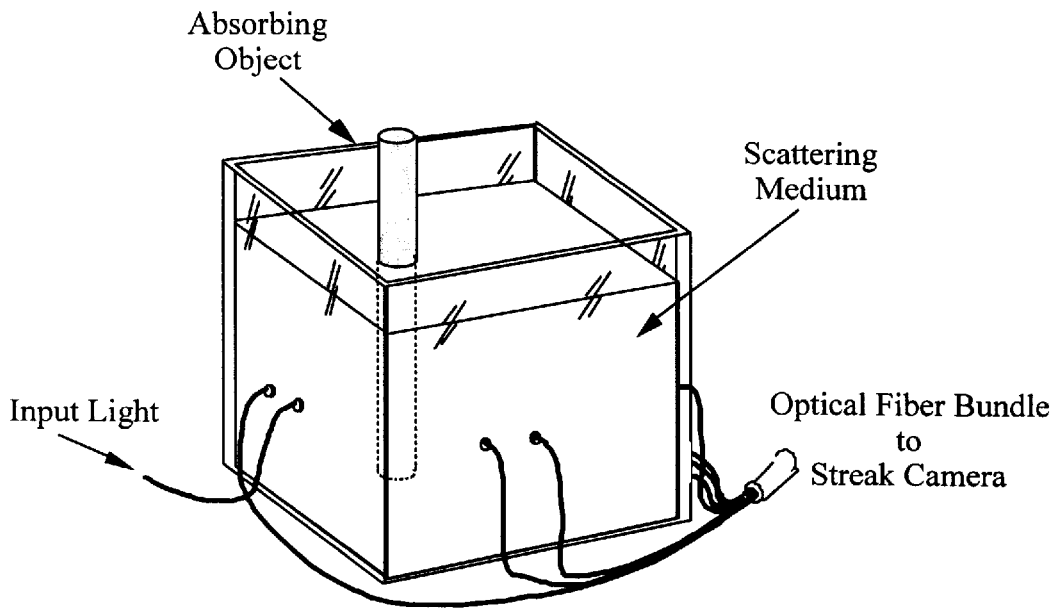


Fig. 1(a)

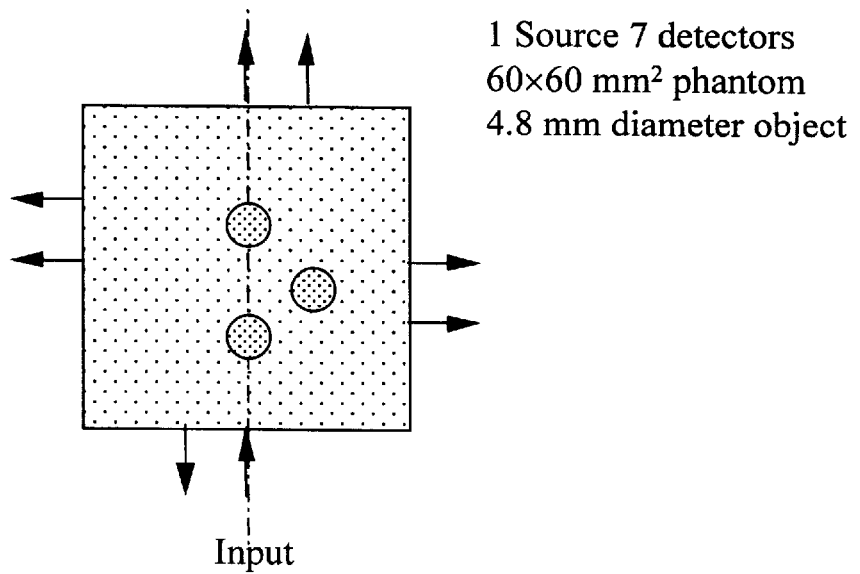


Fig. 1(b)

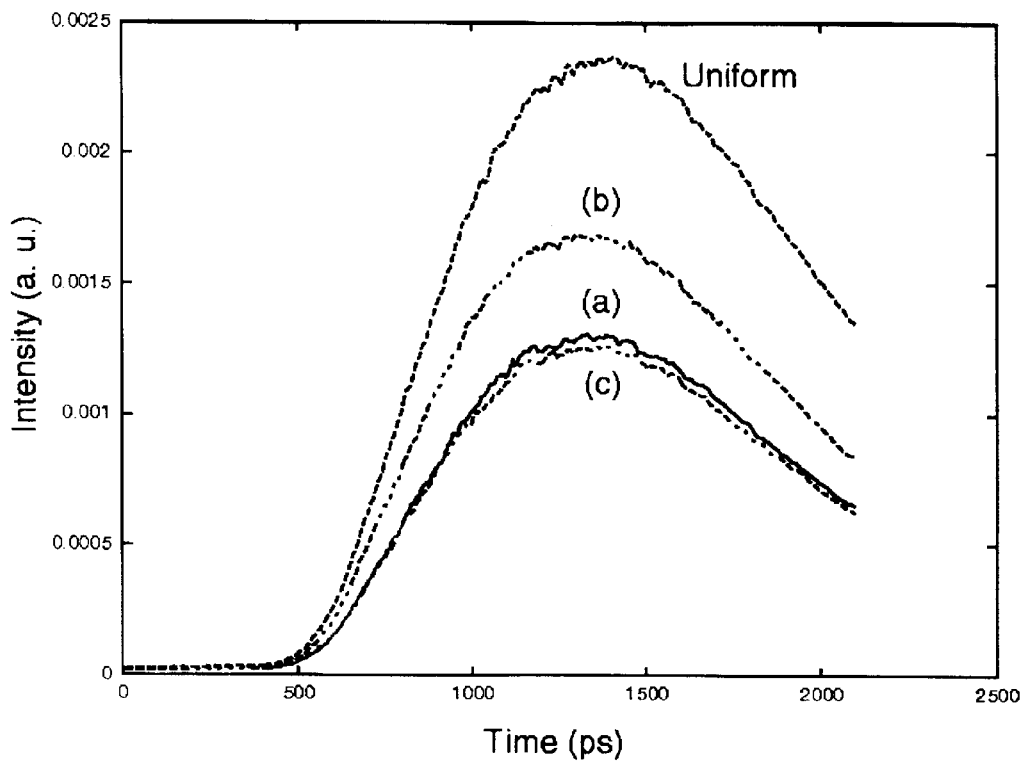


Fig. 2

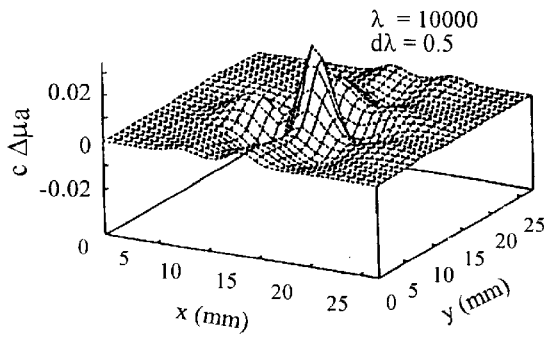


Fig. 3 (a)

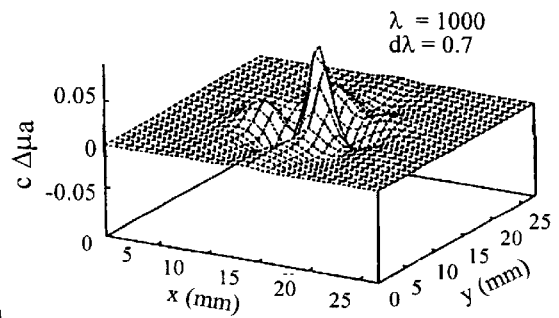


Fig. 3 (b)

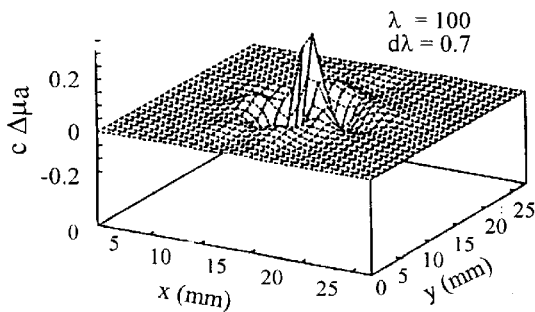


Fig. 3 (c)

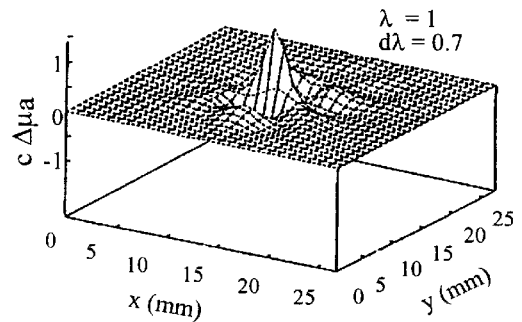


Fig. 3 (d)

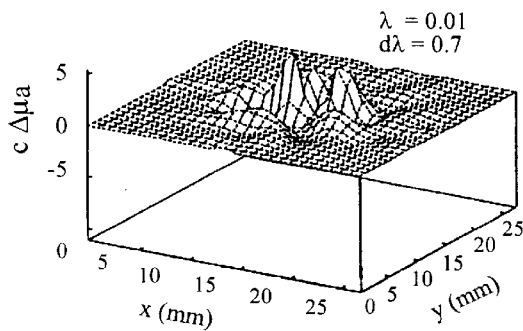


Fig. 3 (e)

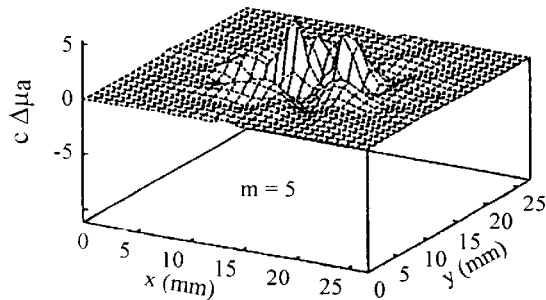


Fig. 4(a)

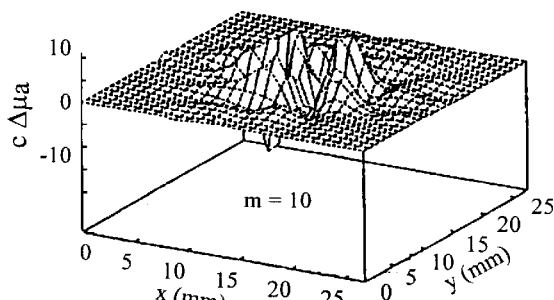


Fig. 4(b)

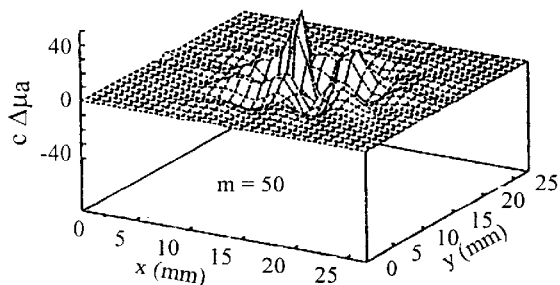


Fig. 4(c)

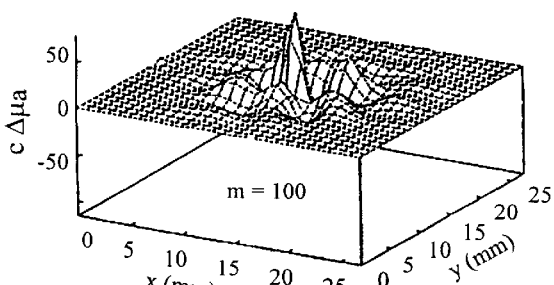


Fig. 4(d)

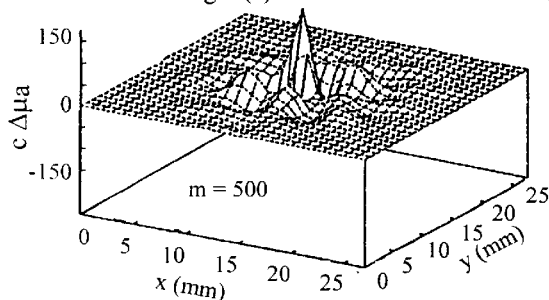


Fig. 4(e)

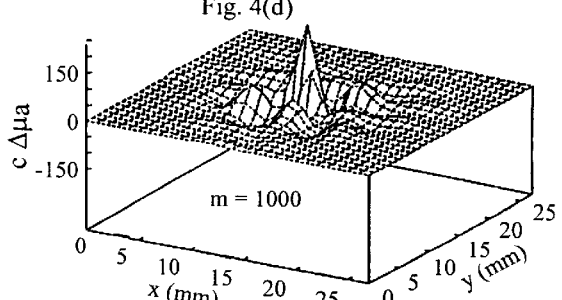


Fig. 4(f)

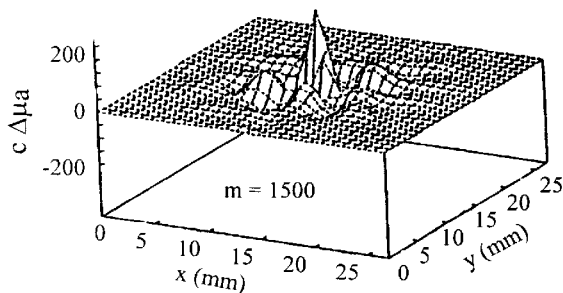


Fig. 4(g)

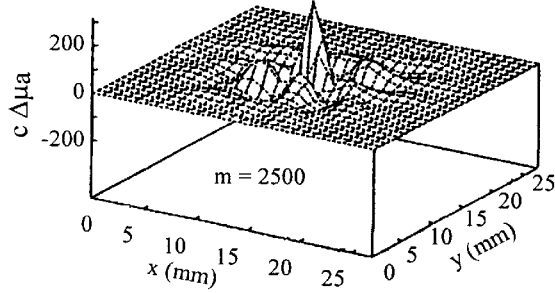
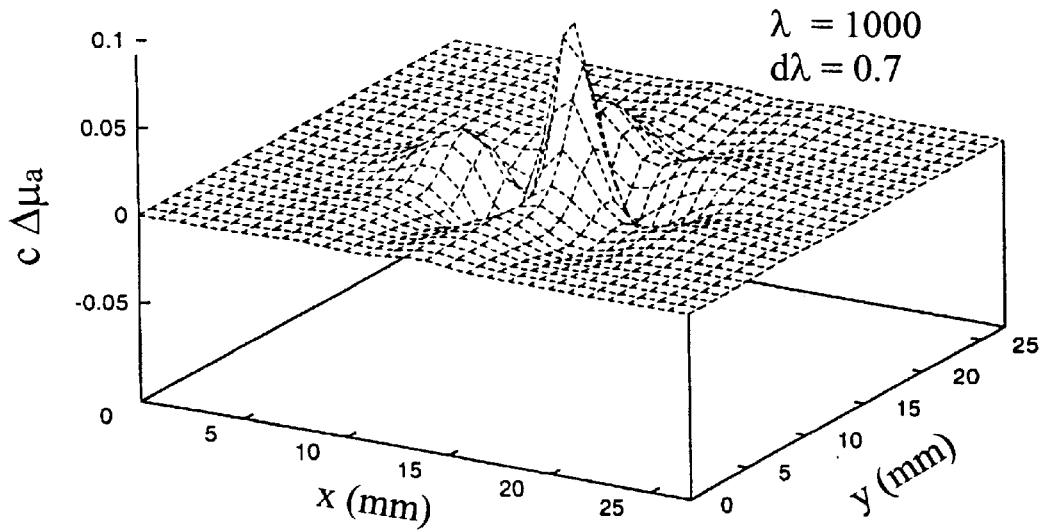
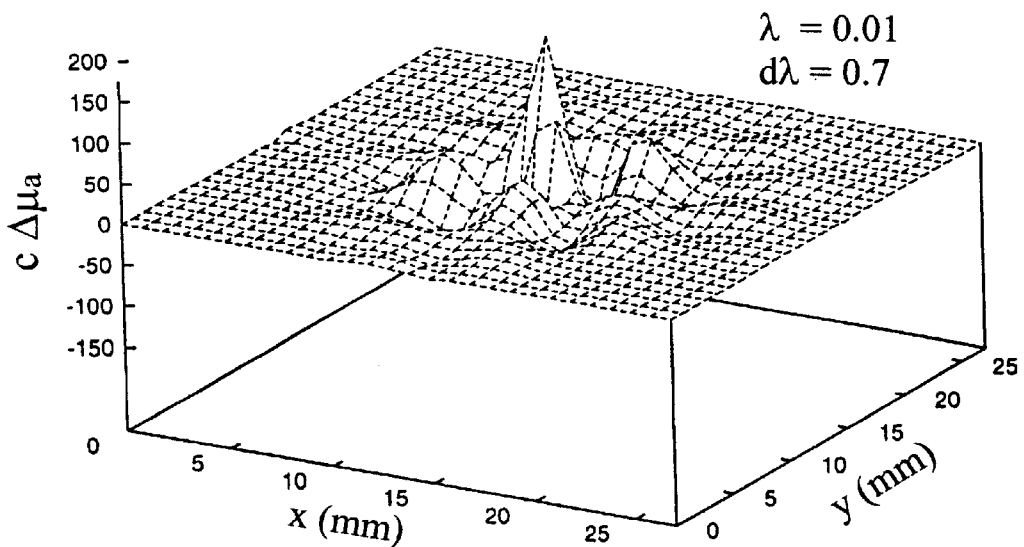


Fig. 4(h)



Without iteration; Running time: 1 minute on SGI Indy computer

Fig. 5(a)



Iteration $m=2000$; Running time: 3 hours on SGI Indy computer

Fig. 5(b)

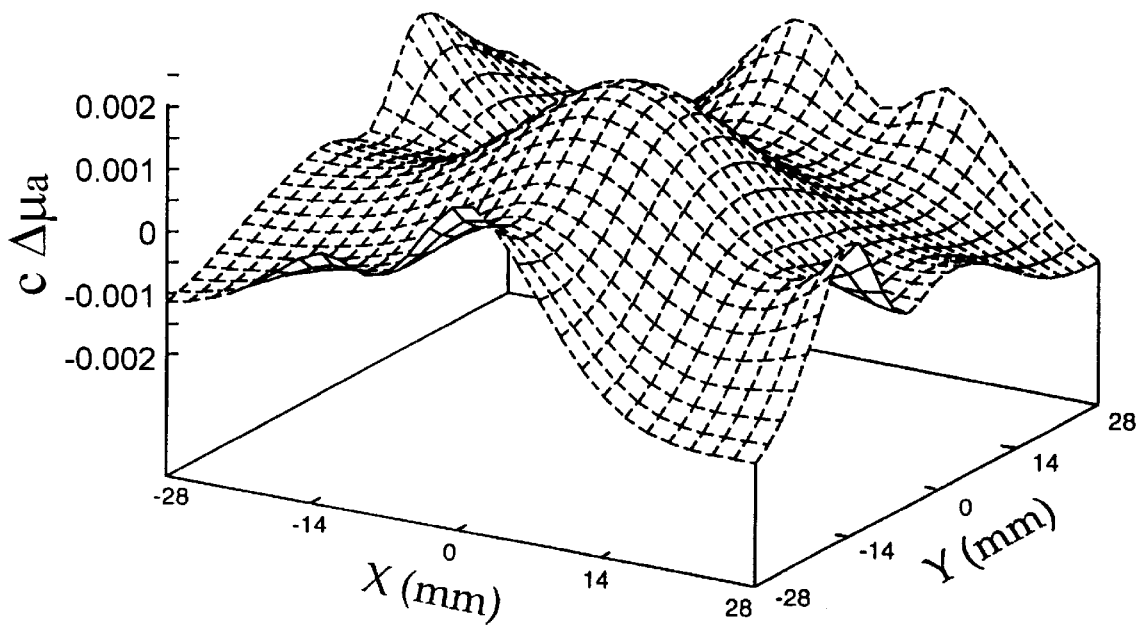


Fig. 6

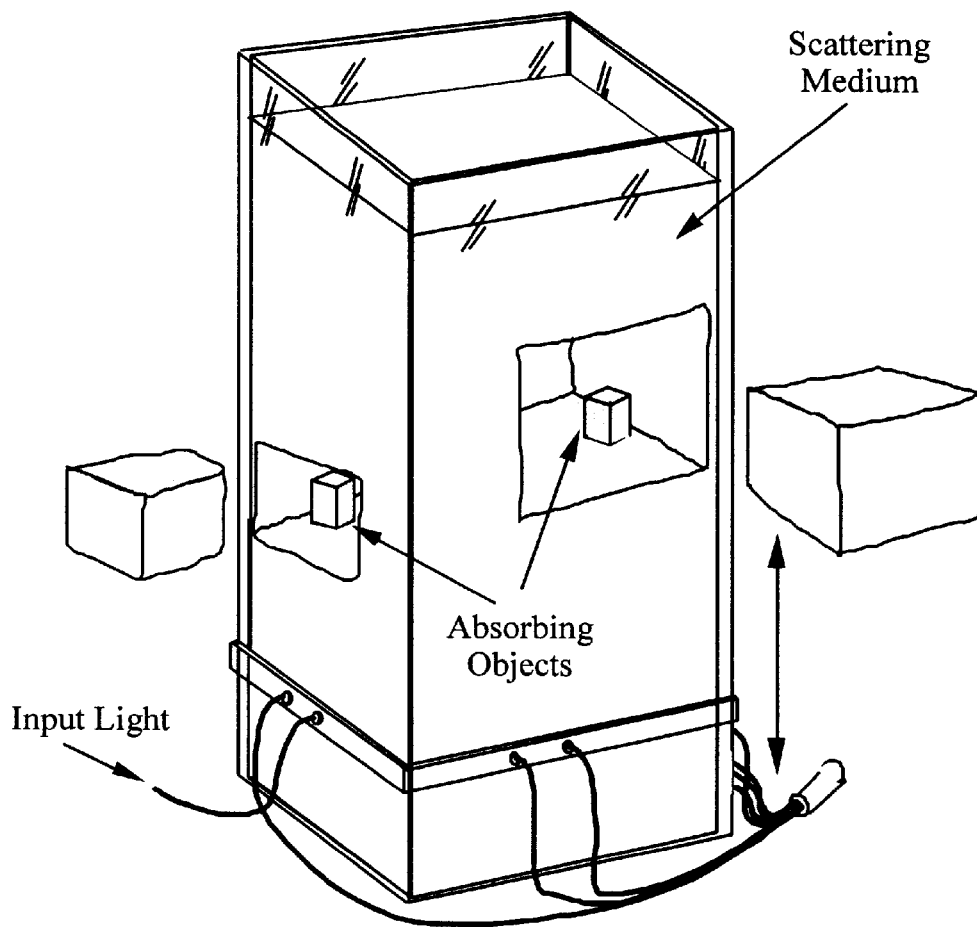


Fig. 7(a)

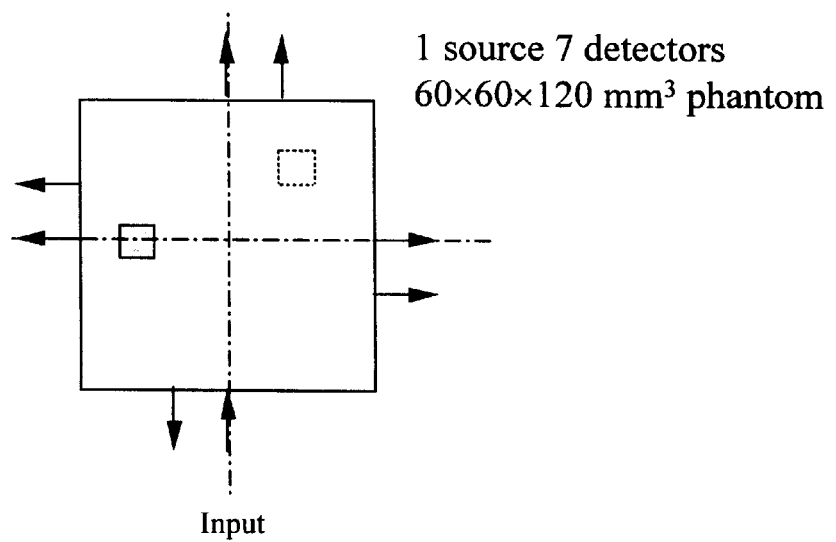
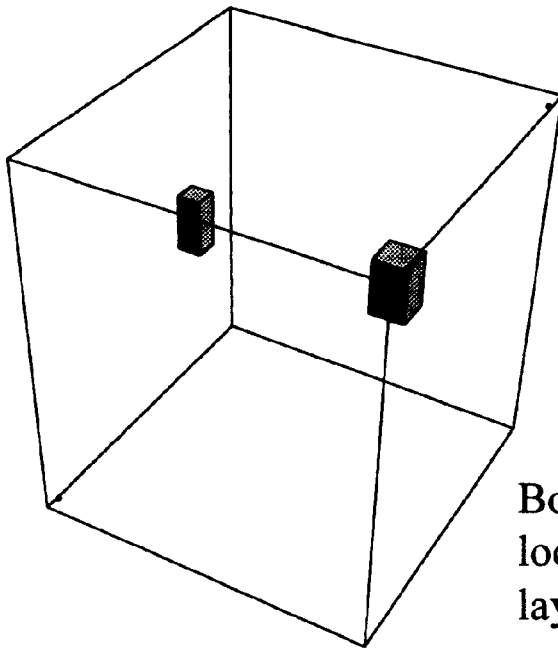
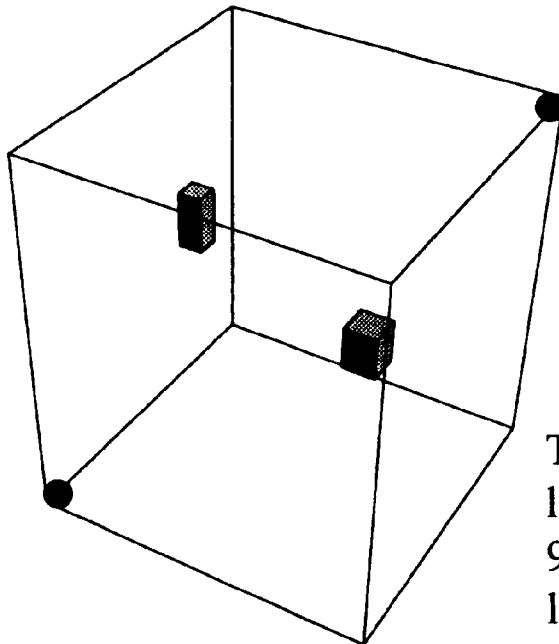


Fig. 7(b)



Both objects are located on z layers 9-13.

Fig. 8(a)



The left objects is located on z layers 9-13, the right object is located on z layers 17-20.

Fig. 8(b)

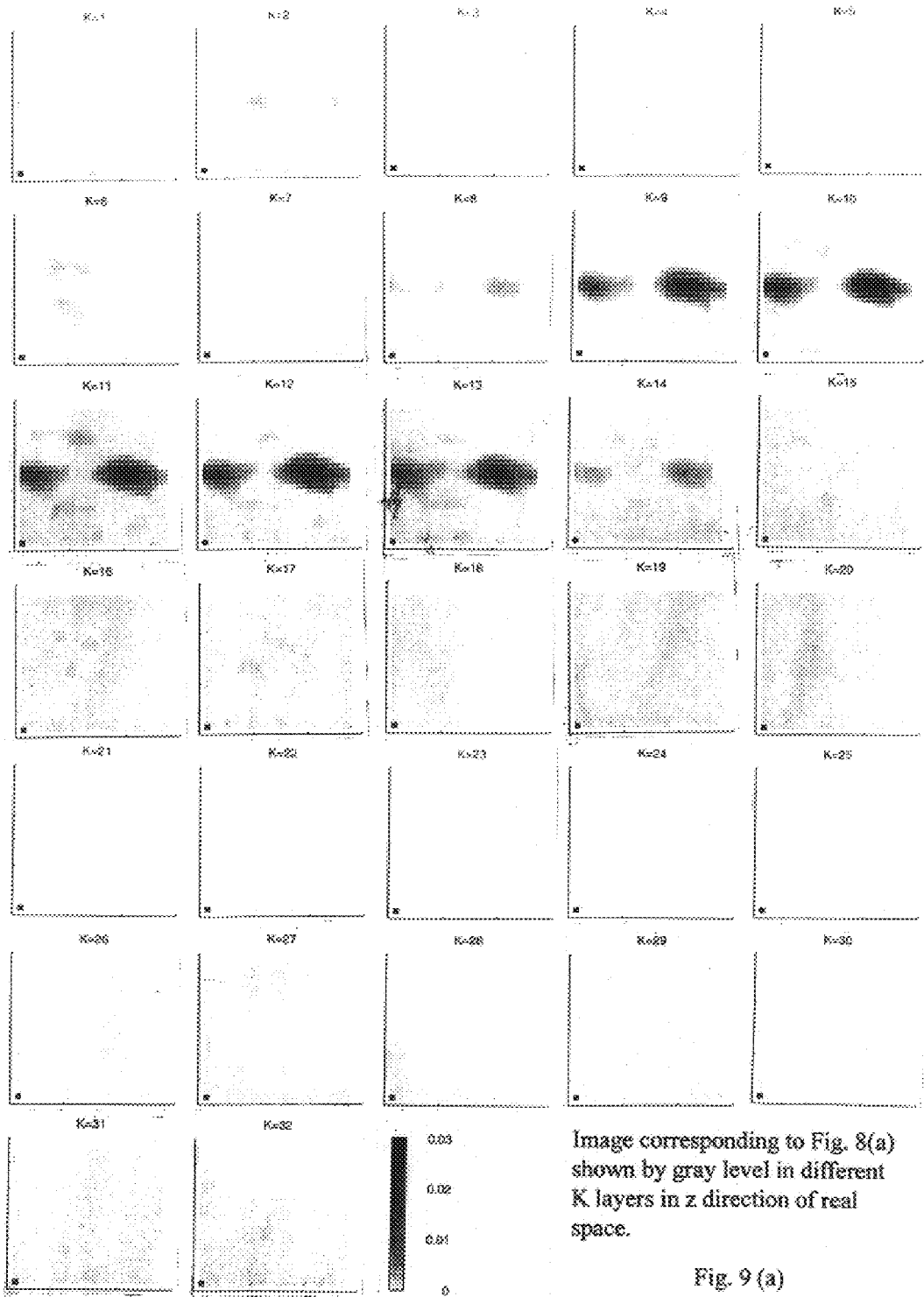


FIG. 9

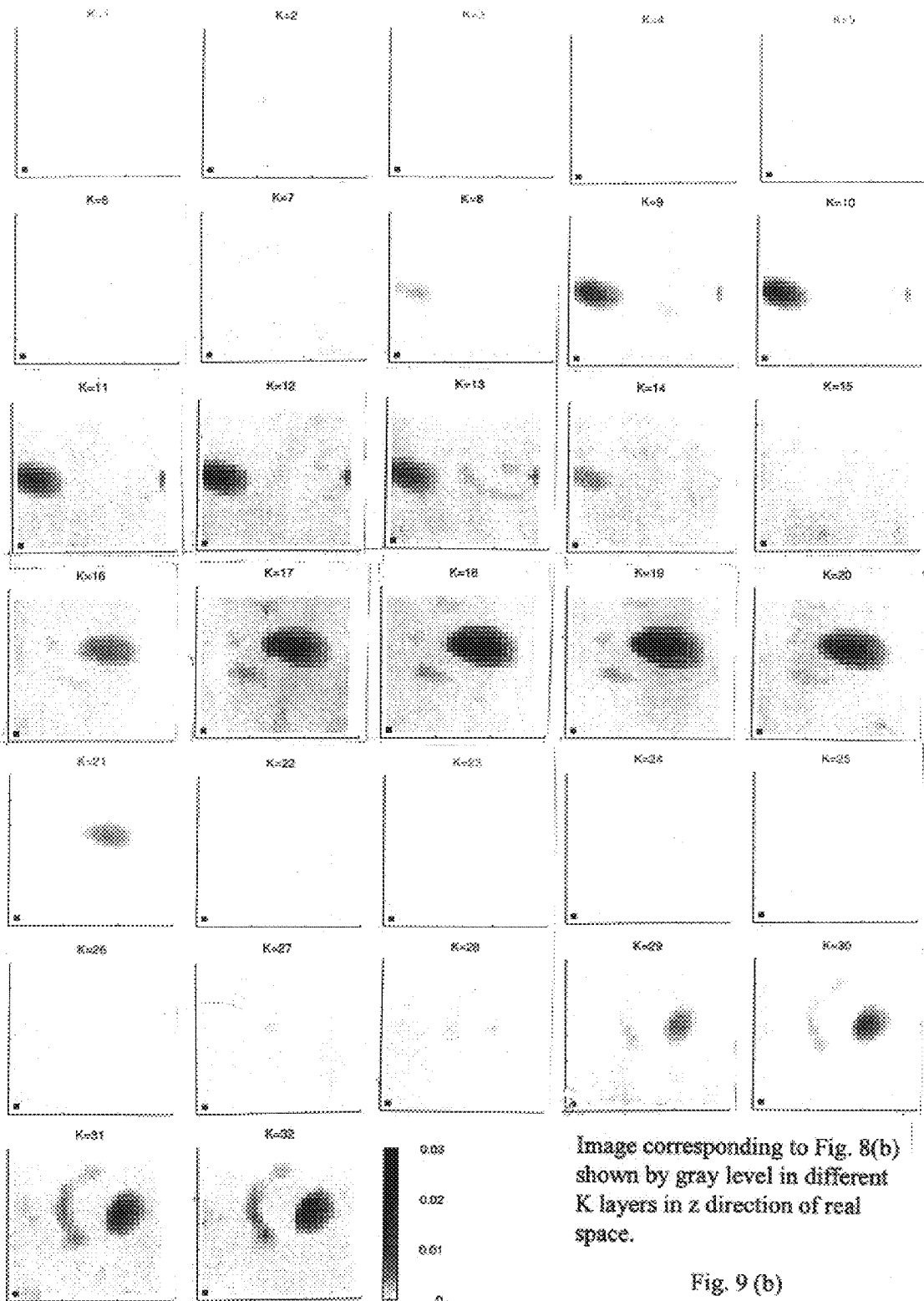


Image corresponding to Fig. 8(b) shown by gray level in different K layers in z direction of real space.

Fig. 9 (b)

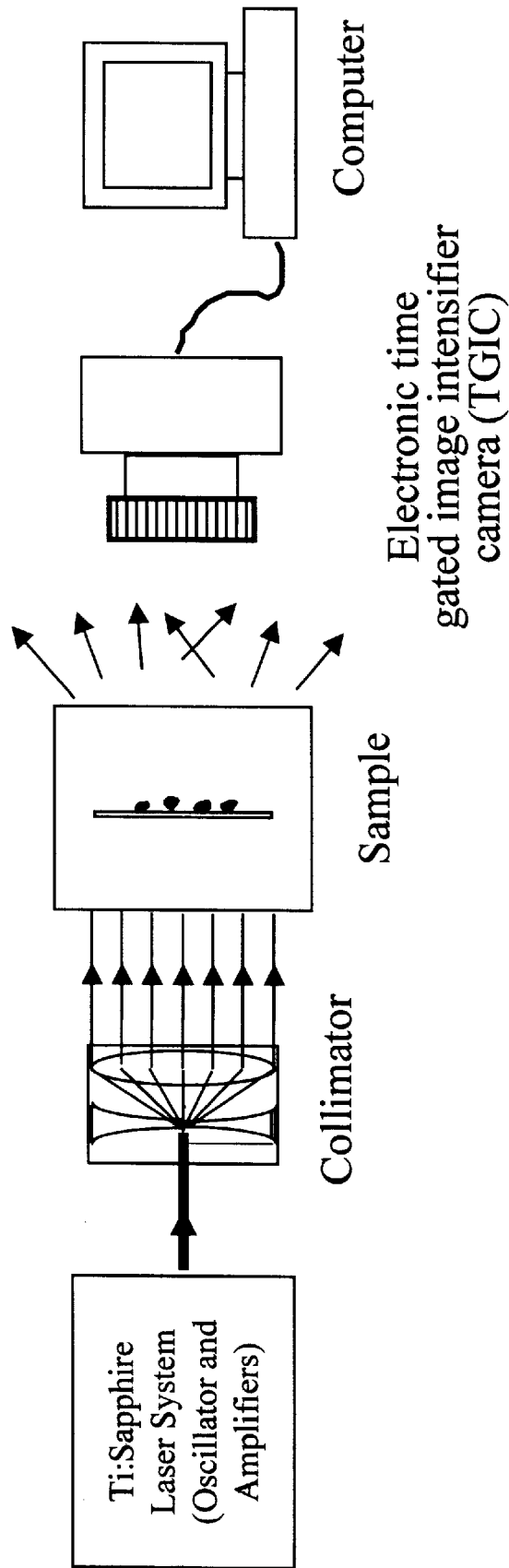


Fig. 10(a)

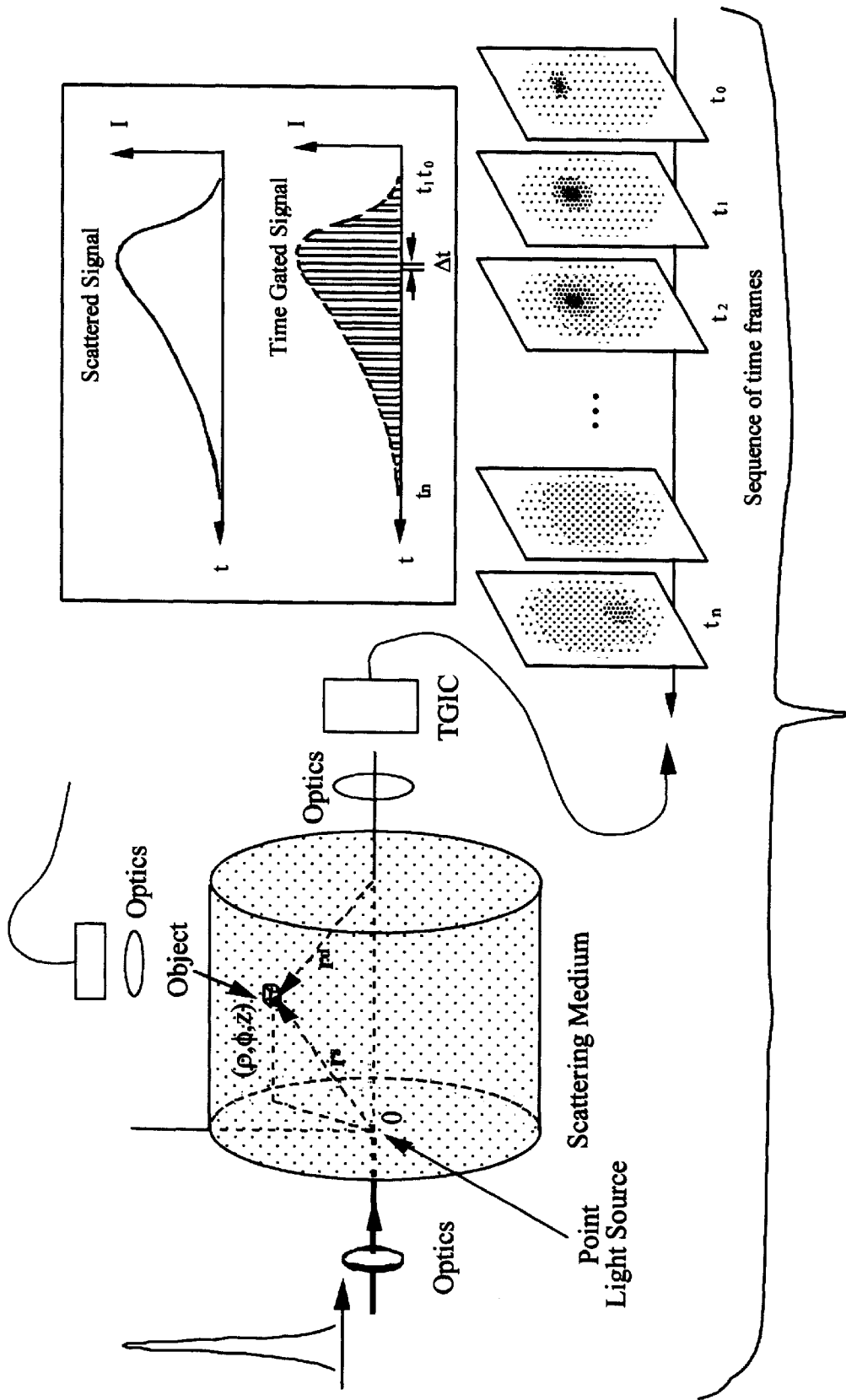


Fig. 10 (b)

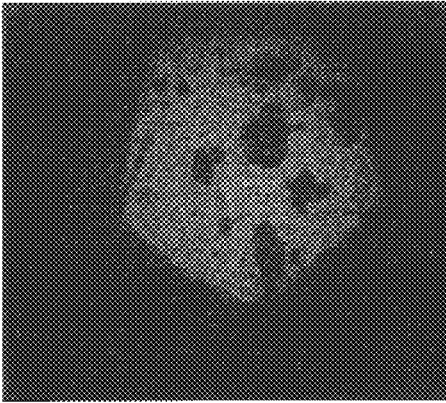


Fig. 11(a)

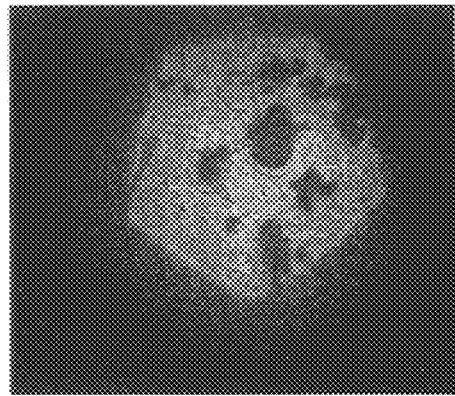


Fig. 11(b)

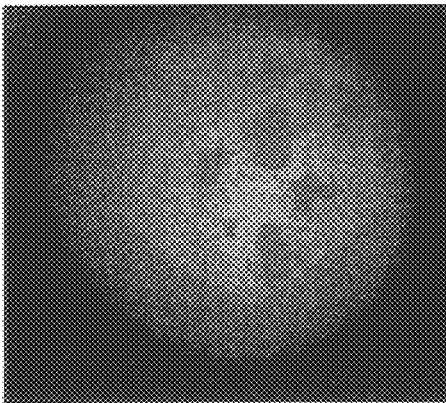


Fig. 11(c)

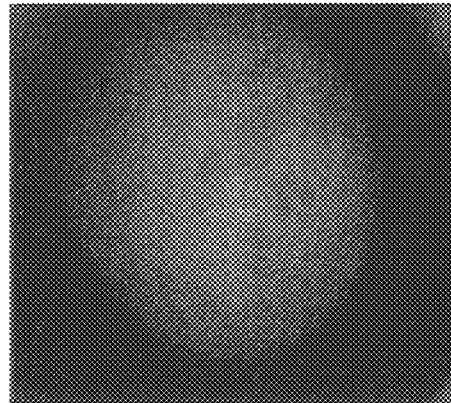


Fig. 11(d)

**TIME-RESOLVED DIFFUSION
TOMOGRAPHIC 2D AND 3D IMAGING IN
HIGHLY SCATTERING TURBID MEDIA**

**CROSS-REFERENCE TO RELATED
APPLICATIONS**

The present application is a continuation-in-part of a pending U.S. patent application Ser. No. 08/797,028, filed Feb. 7, 1997 in the names of Robert R. Alfano, Wei Cai, Feng Liu, Melvin Lax and Bidyut B. Das and entitled TIME-RESOLVED DIFFUSION TOMOGRAPHIC 2D AND 3D IMAGING IN HIGHLY SCATTERING TURBID MEDIA, which in turn is a continuation-in-part of pending U.S. patent application Ser. No. 08/618,471, filed Mar. 18, 1996, both of which is incorporated herein by reference.

**STATEMENT AS TO RIGHTS TO INVENTIONS
MADE UNDER FEDERALLY-SPONSORED
RESEARCH AND DEVELOPMENT**

This invention was made, in part, with Government support awarded by NASA and ONR. The Government may have certain rights in this invention.

BACKGROUND OF THE INVENTION

The present invention relates generally to the imaging of objects in highly scattering turbid media and more particularly to a novel technique for imaging objects in highly scattering turbid media.

As can readily be appreciated, there are many situations in which the detection of an object present in a highly scattering turbid medium is highly desirable. For instance, the detection of a tumor embedded within a tissue is one such example. Although X-ray techniques do provide some measure of success in detecting objects in turbid media, they are not well-suited for detecting very small objects, e.g., tumors less than 1 mm in size, or for detecting objects in thick media. In addition, X-ray radiation can present safety hazards to a person exposed thereto.

An alternative technique used to detect objects in turbid media is transillumination. In transillumination, visible or near infrared (NIR) light is incident on one side of a medium and the light emergent from the opposite side of the medium is used to form an image. Objects embedded in the medium typically absorb the incident light and appear in the image as shadows. Unfortunately, the usefulness of transillumination as a detection technique is severely limited in those instances in which the medium is thick or the object is very small. This is because light scattering within the medium contributes to noise and reduces the intensity of the unscattered light used to form the image shadow.

To improve the detectability of small objects located in a turbid medium using transillumination, many investigators have attempted to selectively use only certain components of the transilluminating light signal. This may be done by exploiting the properties of photon migration through a scattering medium. Photons migrating through a turbid medium have traditionally been categorized into three major signal components: (1) the ballistic (coherent) photons which arrive first by traveling over the shortest, most direct path; (2) the snake (quasi-coherent) photons which arrive within the first δt after the ballistic photons and which deviate, only to a very slight extent, off a straight-line propagation path; and (3) the diffusive (incoherent) photons which experience comparatively more scattering than do ballistic and snake photons and, therefore, deviate more

considerably from the straight-line propagation path followed by ballistic and snake photons.

Because it has been believed that ballistic and snake photons contain the least distorted image information and that diffusive photons lose most of the image information, efforts to make transillumination work most effectively with turbid media have focused on techniques which permit the selective detection of ballistic and snake photons while rejecting diffusive photons. This process of selection and rejection has been implemented in various time-gating, space-gating and time/space-gating techniques. Patents, patent applications and publications which disclose certain of these techniques include U.S. Pat. No. 5,140,463, inventors Yoo et al., which issued Aug. 18, 1992; U.S. Pat. No. 5,143,372, inventors Alfano et al., which issued Aug. 25, 1992; U.S. Pat. No. 5,227,912, inventors Ho et al., which issued Jul. 13, 1993; U.S. Pat. No. 5,371,368, inventors Alfano et al., issued Dec. 6, 1994; Alfano et al., "Photons for prompt tumor detection," *Physics World*, pp. 37-40 (January 1992); Wang et al., "Ballistic 2-D Imaging Through Scattering Walls Using an Ultrafast Optical Kerr Gate," *Science*, Vol. 253, pp. 769-771 (Aug. 16, 1991); Wang et al., "Kerr-Fourier imaging of hidden objects in thick turbid media," *Optics Letters*, Vol. 18, No. 3, pp. 241-243 (Feb. 1, 1993); Yoo et al., "Time-resolved coherent and incoherent components of forward light scattering in random media," *Optics Letters*, Vol. 15, No. 6, pp. 320-322 (Mar. 15, 1990); Das et al., "Ultrafast time-gated imaging in thick tissues: a step toward optical mammography," *Optics Letters*, 18(13):1092-4 (1993); Chen et al., "Two-dimensional imaging through diffusing media using 150-fs gated electronic holography techniques," *Optics Letters*, Vol. 16, No. 7, pp. 487-489 (Apr. 1, 1991); Duncan et al., "Time-gated imaging through scattering media using stimulated Raman amplification," *Optics Letters*, Vol. 16, No. 23, pp. 1868-1870 (Dec. 1, 1991), all of which are incorporated herein by reference.

Of the above-listed art, Wang et al., "Kerr-Fourier imaging of hidden objects in thick turbid media," *Optics Letters*, Vol. 18, No. 3, pp. 241-243 (Feb. 1, 1993) is illustrative of transillumination techniques which selectively use the ballistic and/or snake components of light. In this article, there is disclosed a time/space-gating system for use in imaging opaque test bars hidden inside a 5.5 cm-thick 2.5% Intralipid solution. The disclosed system includes three main parts: a laser source, an optical Kerr gate and a detector. The laser source is a picosecond mode-locked laser system, which emits a 1054 nm, 8 ps laser pulse train as the illumination source. The second harmonic of the pulse train, which is generated by transmission through a potassium dihydrate phosphate (KDP) crystal, is used as the gating source. The illumination source is sent through a variable time-delay and is then used to transilluminate, from one side, the turbid medium containing the opaque object. The signal from the turbid medium located at the front focal plane of a lens is collected and transformed to a Kerr cell located at its back focal plane (i.e., the Fourier-transform spectral plane of a 4F system). That portion of the Kerr cell located at the focal point of the 4F system is gated at the appropriate time using the gating source so that only the ballistic and snake components are permitted to pass therethrough. The spatial-filtered and temporal-segmented signal is then imaged by a second lens onto a CCD camera.

Although techniques of the type described above, which selectively use ballistic and snake photons to image objects in turbid media, have enjoyed a modicum of success, such techniques have been limited by the fact that detected light

signals derived from ballistic and snake photons are typically rather weak, due to the proportionately small number of transilluminated ballistic and snake photons. This problem is further exacerbated in those instances in which the turbid medium is thick and the likelihood of substantial scattering increases.

Accordingly, because diffusive photons constitute the greatest component of the transilluminated light signal, it would be highly desirable to make use of the diffusive component of the light signal in forming an image via transillumination. This objective is made difficult, however, by the fact that diffusive photons tend to traverse a medium along ill-defined paths. One approach to this problem has been to invert the experimental scattering data obtained from various points in the medium using some inverse algorithm and reconstruction approach. This approach is often called diffusion tomography since diffusion or scattering is the dominant factor in the problem. In diffusion tomography, one produces an internal map of the scattering medium using the scattered signals and a mathematical inversion algorithm. The inversion is based upon the physical and mathematical principles governing photon propagation in turbid media. Both time-resolved data and frequency domain data can be used for reconstruction. Examples of diffusion tomography techniques include Arridge, "The Forward and Inverse Problems in Time Resolved Infra-Red Imaging," *Medical Optical Tomography: Functional Imaging and Monitoring SPIE Institutes*, Vol. IS11, G. Muller ed., 31–64 (1993); Singer et al., "Image Reconstruction of the Interior of Bodies That Diffuse Radiation," *Science*, 248:990–3 (1993); Barbour et al., "A Perturbation Approach for Optical Diffusion Tomography Using Continuous-Wave and Time-Resolved Data," *Medical Optical Tomography: Functional Imaging and Monitoring SPIE Institutes*, Vol. IS11, G. Muller ed., 87–120 (1993); M. Patterson et al., *SPIE*, 1767, 372 (1992); J. Schotland et al., *App. Opt.*, 32, 448 (1993), all of which are incorporated herein by reference.

The foregoing diffusion tomography techniques do not lead to a resolution that is better than about 5–10 mm. Moreover, these techniques are time-consuming and do not readily lend themselves to real-time use.

SUMMARY OF THE INVENTION

It is an object of the present invention to provide a novel technique for imaging objects present in highly scattering turbid media.

It is another object of the present invention to provide a technique as described above that overcomes at least some of the disadvantages associated with existing techniques for imaging objects in highly scattering turbid media.

Additional objects, as well as features and advantages, of the present invention will be set forth in part in the description which follows, and in part will be obvious from the description or may be learned by practice of the invention.

The present invention is based on the present inventors' discovery that objects hidden in highly scattering turbid media can be imaged by a novel, fast and noise-resistant inverse method which involves illuminating a highly scattering turbid medium with a pulse of light, the light emergent from the highly scattering turbid medium consisting of a ballistic component, a snake-like component and a diffusive component; determining the intensity of said diffusive component at a plurality of points in time; and using said intensity determinations to form an image of the object in the highly scattering turbid medium.

The aforementioned illuminating and determining steps preferably include the use of a light source and one or more

detectors, said detectors preferably including means, such as a streak camera, for temporally resolving the diffusive component of the emergent light from the highly scattering turbid medium. More preferably, two or more source/detector sets are arranged in an intersecting manner to enable a 2-D or 3-D image to be formed.

The aforementioned illuminating and determining steps more preferably include the use of one or more two-dimensional area detectors, such as a charge-coupled device (CCD) or an infrared area camera. The detectors preferably include means to amplify the emergent light pulse from the turbid medium and to carve out any desired temporal slice of the pulse. The output of the detector is a shadow-image or a two-dimensional time-dependent intensity distribution, $I(x,y,t)$, where the direction of incidence of light pulse is taken to be along the z direction. One such detector configuration comprises a gated image intensifier coupled to a CCD camera. This particular detection and imaging scheme is a specific embodiment of the electronic time-gating technique and will hereinafter be referred to as an electronic time-gated imaging camera (TGIC) system. The duration and the position of the gate is variable from a few picoseconds to a few nanoseconds. Such a system presently used by the inventors provides a minimum gate duration of 80 ps. The gate position can be varied in 25 ps steps.

Preferably, the following inverse reconstruction algorithm is used to form an image of the turbid medium using the aforementioned intensity determinations:

$$X^{(k+1)T} = [Y^T W + X^{(k)T} \Lambda] [W^T W + \Lambda]^{-1}$$

wherein W is a matrix relating output at source and detector positions r_s and r_d at time t to input at a voxel's position r , Λ is a regularization matrix, chosen for convenience to be diagonal but selected in a way related to the ratio of the noise, $\langle nn \rangle$ to fluctuations in the absorption (or diffusion) X_j that we are trying to determine:

$$\Lambda_{ij} = \lambda_j \delta_{ij} \text{ with } \lambda_j = \langle nn \rangle / \langle \Delta X_j \Delta X_j \rangle$$

Y is the data collected at the detectors, and X^k is the k th iterate toward the desired absorption information.

A distinct advantage of the present method, over existing inverse reconstruction methods for imaging objects located in highly scattering turbid media using diffusive photons, is that the present method can be done with fewer iterations, thereby making possible real-time imaging.

An inverse algorithm, which combines a two dimensional (2D) matrix inversion with a one-dimensional (1D) Fourier transform inversion, is also disclosed herein to obtain images of three-dimensional (3D) objects hidden in turbid scattering media. To obtain such 3D images, the source-detector pairs are arranged in a 2D plane (the x - y plane), which are scanned along the z direction. Data is obtained from S-D pairs at z positions for processing. The reference system is assumed to be uniform and infinite along the z direction. In the above experimental setting, the weight function, W , satisfies translation invariance. In other words, it is a function of $z-z_0$, where z_0 is the z -position of source-detector plane and z is z -coordinate of a voxel.

After making a one-dimensional Fourier transform of W over $z-z_0$, we obtain K independent 2D matrices, $W_{2D}(k)$, parameterized by k , with K the number of grid-points in the Fourier k -space. We separately calculate the K inverse matrices $[W_{2D}(k) + \Lambda(k)]^{-1}$, $k=1,2,3, \dots, K$, where $\Lambda(k)$ is a matrix for regularization. These inverse matrices

are stored as a database for later reconstruction of the image in different hidden object cases.

Experimental data in time-resolved (or frequency domain) are $Y(r_d, r_s, t(\omega), z_0)$, where r_d and r_s are (x,y) coordinates of detector and source, t is the time slice (or ω is frequency). We make a Fourier transform over z_0 to obtain $Y(r_d, r_s, t(\omega), k)$, $k=1,2,3, \dots, K$. We then calculate the image in the k space using the following matrix multiplication:

$$X(k)=Y(k)^T W_{2D}(k) [W_{2D}(k)^T W_{2D}(k) + \Lambda(k)]^{-1}, k=1,2,3, \dots, K$$

Then, the inverse 1D Fourier transform of $X(k)$ over k generates the 3D distribution of the change of absorption coefficients or scattering coefficients.

The aforementioned method of 3D imaging using matrix inversion and Fourier transform greatly reduces the computational burden compared to standard 3D matrix inversion methods, while maintaining mathematical integrity in the use of Fourier Transform.

To demonstrate the capacity of the above-described method, we used said method to obtain a 3D image with $28 \times 28 \times 32$ voxels. An image was reconstructed by running about 30 minutes on a Silicon Graphic Indy 4400 computer for 3D. In this manner, the data may be taken and the image calculated while a patient waits for results.

The present invention is also directed to systems constructed in accordance with the foregoing methods.

In the description which follows, reference is made to the accompanying drawings which form a part thereof and in which is shown by way of illustration specific embodiments for practicing the invention. These embodiments will be described in sufficient detail to enable those skilled in the art to practice the invention, and it is to be understood that other embodiments may be utilized and that structural changes may be made without departing from the scope of the invention. The following detailed description is, therefore, not to be taken in a limiting sense, and the scope of the present invention is best defined by the appended claims.

BRIEF DESCRIPTION OF THE DRAWINGS

The accompanying drawings, which are hereby incorporated into and constitute a part of this specification, illustrate various embodiments of the invention and, together with the description, serve to explain the principles of the invention. In the drawings wherein like reference numerals represent like parts:

FIGS. 1(a) and 1(b) are simplified schematic perspective and section views, respectively, of an experimental setup used to test the imaging method of the present invention;

FIG. 2 is a graphic representation of various time-resolved curves obtained using the experimental setup of FIGS. 1(a) and 1(b), curves (a) through (c) being obtained by positioning an object in the three locations (a), (b) and (c), respectively, of FIG. 1(b), and the curve labelled "Uniform" being obtained by not positioning the object within the sample medium;

FIGS. 3(a) through 3(e) are comparative images of the object of FIG. 1(a) obtained using the method of the present invention with different regularization parameters;

FIGS. 4(a) through 4(h) are comparative images of the object of FIG. 1(a) obtained using the method of the present invention with different numbers of iterations;

FIGS. 5(a) and 5(b) are comparative images of the object of FIG. 1(a) obtained using the method of the present invention with (a) a comparatively great degree of regularization and no iteration; and (b) a comparatively low degree of regularization and 2000 iterations, respectively;

FIG. 6 is an image of the object of FIG. 1(a) obtained using the conventional Simultaneous Algebraic Reconstruction Technique (SART) after 3 hours and 100 iterations;

FIGS. 7(a) and 7(b) are schematic views of an experimental setup used to generate a 3D image of two objects hidden in a scattering medium;

FIGS. 8(a) and 8(b) are schematic representations of two different arrangements of a pair of 3D objects hidden in a scattering medium;

FIG. 9(a) represents a series of images of the objects of FIG. 8(a) shown at different places in the z direction;

FIG. 9(b) represents a series of images of the objects of FIG. 8(b) shown at different places in the z direction;

FIG. 10(a) is a simplified schematic diagram of an experimental arrangement used to implement the imaging method of the present invention, the arrangement using an electronic time-gating technique with a gated image intensifier and a CCD camera;

FIG. 10(b) is a simplified schematic diagram of a sample-cell arrangement used to accompany the imaging arrangement of FIG. 10(a). Also presented is a schematic diagram of a sequence of shadowgram-like images that are two-dimensional intensity distributions as a function of gate delay, $I(x,y,t)$. Integrated intensity over the same small area of all the shadow images in the sequence plotted as a function of gate position generates a temporal intensity profile, also displayed in FIG. 10(b) above the sequence of image frames. Temporal intensity profiles may also be obtained by plotting the average intensity over a small area or the intensity value at a particular point on the shadow images as a function of gate position; and

FIG. 11 shows a sequence of four shadow images measured with the electronic time-gated imaging camera system of the present invention, the frames (a), (b), (c) and (d) corresponding to images taken at gate positions of -50 , 0 , 50 and 100 ps, respectively, with respect to the ballistic pulse.

DETAILED DESCRIPTION OF PREFERRED EMBODIMENTS

As indicated above, the present invention is based upon the present inventors' discovery that objects hidden in highly scattering turbid media can be imaged by a novel, fast and noise-resistant inverse method which comprises, among other things, transilluminating a highly scattering turbid medium using a plurality of intersecting source-detector pairs and using intensity measurements of the diffusive component of the detected light signals taken over a plurality of time windows (or "time-slices") in a novel inverse reconstruction algorithm.

The following discussion provides the theoretical basis for the present invention: A scattered signal is, in general, a function of key parameters characterizing the medium. The forward problem is to build a mathematical model that allows computation of signals when a spatial distribution of key parameters is given. This mathematical model is clearly based on the fundamental physical principles governing the interaction. The inverse problem is to find the distribution of these key parameters that best fit the given signal data. For photon propagation in turbid media, the key parameters characterizing the interaction are the absorption length, the transport mean free path, the scattering mean free path, and the index of refraction of media. The parameters are in general functions of position (\vec{r}) and wavelength (λ). In the case of optical diffusion tomography, the most commonly used key parameters are absorption and transport scattering

coefficients, which are the inverse of absorption length and transport scattering mean free path, respectively. The mathematical model governing the photon propagation is the photonic transport theory or its approximations, such as the diffusion theory or the telegrapher's equation.

To show the basic principle of this technique, diffusion theory is applied here to model light propagation in turbid media. The diffusion equation in turbid media is

$$\left[\frac{\partial}{\partial t} + c\mu_a(\vec{r}) - \nabla(cD(\vec{r})\nabla) \right] I(\vec{r}, t) = S(\vec{r}, t) \quad (1)$$

where $I(\vec{r}, t)$ is the field of photon density, $S(\vec{r}, t)$ is the source of laser light, μ_a is the absorption coefficient, $D=1/[3(\mu_a+(1-g)\mu_s)]$ is the diffusion coefficient, with μ_s the scattering coefficient, g the scattering anisotropic factor and c the speed of light in the medium.

We are interested in the following problem: given intensity measurements taken around the media either with objects located therein, $I(\vec{r}, t)$, or without objects located therein, $I_0(\vec{r}, t)$, reconstruct a spatial map of the change in optical parameters (absorption and diffusion coefficients) due to the presence of hidden objects.

The forward problem of scattering can be represented in a matrix form written as

$$Y=WX+n \quad (2)$$

where Y has $M=(\text{number of S-D pairs}) \times (\text{number of time slices})$ elements, which is the change in intensity profile and is a function of the position of source \vec{r}_s , the position of detector \vec{r}_d , and the time-slice in the profile t . X has $N=(\text{number of voxel})$ elements wherein a voxel is a space grid element. $X_j=c\Delta\mu_a(\vec{r}_j)$ or $c\Delta D(\vec{r}_j)$ is the (time-independent) change in the absorption coefficient or the diffusion coefficient in the voxel j due to the presence of hidden objects, and n is signal detector noise. W is an $M \times N$ matrix. Its element is the weight function or "photon measurement density functions." This weight function represents the change in signal at the detector placed at \vec{r}_d at time t from a source signal originating at \vec{r}_s associated with a unit change in absorption coefficient (or diffusion coefficient) at \vec{r}_j of the reference medium, as implemented by a diffusion process that carries the signal from source at \vec{r}_s to the detector at \vec{r}_d . Its value is theoretically calculated according to the mathematical model, for example, the diffusion theory in the case shown below.

Using Green's function formula, for the case of absorption change, $c\Delta\mu_a$, the element of W is given by

$$W[(\vec{r}_d, \vec{r}_s, t), \vec{r}_j] = \frac{\Delta V}{G^0(\vec{r}_d, \vec{r}_s, t)} \int_0^t d\tau G^0(\vec{r}_d, \vec{r}_j, t-\tau) G^0(\vec{r}_j, \vec{r}_s, \tau) \quad (3.1)$$

where $G^0(\vec{r}_j, \vec{r}_s, t)$ is the Green's function of Eq.(1) for a reference system (the system with no hidden object) which gives the normalized photon intensity at \vec{r}_j at time t as migrating photons originate from \vec{r}_s at time $t=0$. In Eq.(3.1), the second Green's function in the integral, $G^0(\vec{r}_j, \vec{r}_s, \tau)$ represents the photons that migrate from a source to a given voxel element. The first one, $G^0(\vec{r}_d, \vec{r}_j, t-\tau)$, represents the

photons that migrate from this voxel to a detector. ΔV is volume of a voxel. Therefore, W in Eq.(3.1) represents a normalized effect that photons originating from the source migrate through voxel j , then further migrate to the detector during a total time of t . In the case of diffusion or scattering change, both G^0 in the integral of Eq.(3.1) are replaced by ∇G^0 .

$$W[(\vec{r}_d, \vec{r}_s, t), \vec{r}_j] = \frac{\Delta V}{G^0(\vec{r}_d, \vec{r}_s, t)} \int_0^t d\tau \nabla G^0(\vec{r}_d, \vec{r}_j, t-\tau) \cdot \nabla G^0(\vec{r}_j, \vec{r}_s, \tau) \quad (3.2)$$

One preferred geometry for experiments with the electronic time-gated imaging camera (TGIC) system, shown in FIG. 10(b), requires the use of cylindrical co-ordinate system. The source is located on the origin. The $G^0(r, r_s)$ in Eqs. (3.1) and (3.2) is ϕ independent, and $G^0(r, r_d)$ depends on $(\phi-\phi_d)$, if a cylinder symmetry and a uniform background is assumed. In above experimental setting, the weight function, W , satisfies translational invariance. In other words, it is a function of $(\phi-\phi_d)$, where ϕ_d is the polar angle of detectors and ϕ is the polar angle of a voxel. Therefore, W_{3D} has indices of $\rho_d, t; \rho, z, \phi-\phi_d$, while z_d is fixed.

After making a one-dimensional Fourier transform of W_{3D} over $(\phi-\phi_d)$, we obtain K independent 2D matrices, parameterized by k , with K the number of grid-points in the Fourier k -space. W_{2D} is function of $(\rho_d, t; \rho, z)$. Information on time slices provides an equivalent 1D data for inverse of image on (ρ, z) voxels in k space.

We separately calculate the K inverse matrices $[W_{2D}(k) W_{2D}(k) + \Lambda(k)]^{-1}$, $k=1, 2, 3, \dots, K$, where $\Lambda(k)$ is a matrix for regularization. These inverse matrices are stored as database for later reconstruction of image for different hidden objects.

Experimental time-resolved data are $Y(\rho_d, \phi_d, t)$. We make a Fourier transform over ϕ_d to obtain $Y(\rho_d, t, k)$, $k=1, 2, 3, \dots, K$. We then calculate the image in the k space using the following matrix multiplication:

$$X(k) = Y(k)^T W_{2D}(k) [W_{2D}(k) W_{2D}(k) + \Lambda(k)]^{-1}, \quad k=1, 2, 3, \dots, K \quad (3.3)$$

Then, the inverse 1D Fourier transform of $X(k)$ over k generates the 3D distribution of the change of absorption or scattering coefficients on (ρ, ϕ, z) voxels.

According to certain previously-used inversion algorithms employed in image reconstruction, such as Algebraic Reconstruction Technique (ART), Simultaneous Algebraic Reconstruction Technique (SART) or Conjugate Gradients (CGD), the fractional signal change $Y=-(I-I_0)/I_0$, which corresponds to the first order perturbation, is used. Such inversion reconstruction algorithms, however, generally requires a great number of iterations in order for a clear image map of hidden objects to be obtained. Such iterations frequently can take an amount of calculation time that exceeds the practical time limit for clinical applications.

A more accurate non-perturbative approximation based on a cumulant expansion has been developed by us, which fits the experimental data by $Y=-\ln(I/I_0)$. This treatment, to some extent, automatically includes higher order non-linear contributions. The inversion is a reconstruction of optical parameters from signals. In order to make a fast inversion for clinical applications, we have developed the following novel inverse reconstruction procedure based on a modification of the iteration formula described in Shaw, "Improvement of the Numerical Resolution of An Instrument by Numerical Solution of the Integral Equation," *J. Math.*

Analys. and Applic., 37:83–112 (1972), which is incorporated herein by reference:

$$X^{(k+1)T} = [Y^T W + X^{(k)T} \Lambda] [W^T W + \Lambda]^{-1} \quad (4)$$

where Y , $(-ln(I/I_0))$, is the input data for inversion. $X^{(k)}$ and $X^{(k+1)}$ are k^{th} and $(k+1)^{th}$ iteration solutions, respectively, for the change of parameters. The initial value of X is set to zero in the absence of prior information about hidden objects. T represents the transpose matrix. The matrix Λ , which regularizes or converts an ill-posed problem to a well-posed problem, is chosen to be diagonal, $\Lambda_{ij} = \lambda_j \delta_{ij}$. $\lambda_j = \langle nn \rangle / \langle \Delta X_j \Delta X_j \rangle$, with $\langle \dots \rangle$ the statistical average, and $\Delta X_j = X_j - \langle X_j \rangle$. Thus, λ_j represents the ratio of mean square of noise to the expected mean square deviation in the change of parameters (structural noise).

Since W does not relate to the position and optical parameters of hidden objects, having W for a given reference system (either homogeneous or inhomogeneous), the inverse matrix $[W^T W + \Lambda]^{-1}$ can be precalculated and stored as a database, which can be used in clinical cases to find hidden objects. This strategy separates time-consuming work in inversion processes into two parts. Pre-computation is time-consuming and may require the use of a supercomputer. However, it greatly reduces the burden of performing inverse processes in daily clinical cases.

One of the main difficulties in inversion is that most inverse problems are ill-posed. If no noise existed, an inverse image could be reconstructed from Eq.(2) via: $X^T = Y^T W [W^T W]^{-1}$. The existence of a small amount of noise should not have much effect on the results obtained. However, the matrix $W^T W$ is generally ill-posed or near-singular. In other words, this matrix has some near-zero eigen values. This occurs when the number of measurements M is less than the number of unknown parameters N or when the measured signals are not fully independent of each other. In this case, the effect of small noise will be magnified in the inverse process, and the solution of inversion becomes unstable. One of the methods to overcome the ill-posed problems is regularization, which adds a Λ to the matrix $W^T W$. Λ is relatively small compared to the matrix $W^T W$; therefore, regularization makes the matrix well-posed or well-defined, but does not change the characteristics of the image map. The value of Λ is set according to the experimental noise level and structural noise present in the change of optical parameters. If $\|\Delta W^T W\| < 1$, one may use the following expansion to correct the error introduced by regularization:

$$[W^T W]^{-1} = [B - \Lambda]^{-1} = B^{-1} + B^{-1} \Lambda B^{-1} + B^{-1} \Lambda B^{-1} \Lambda B^{-1} + \dots \quad (5)$$

The iterations in Eq.(4) are equivalent to the above expansion.

If noise n exists, $Y = WX + n$. One wants to find an inverse operator, $\hat{X} = \hat{L}Y$, which gives the estimated value \hat{X} of X , that, in the sense of statistical average, has minimum error. Shaw has derived the following solution:

$$\hat{X} = [Y^T W \langle \Delta X \Delta X \rangle + \langle X \rangle \langle nm \rangle] \times [\langle \Delta X \Delta X \rangle W^T W + \langle nm \rangle]^{-1} \quad (6)$$

with $\langle \dots \rangle$ statistical average, $\Delta X = X - \langle X \rangle$. We see that Eq.(6) is a well-posed expression. This approach is the so-called “well-posed stochastic extension of ill-posed linear processes” or “statistical regularization.” Comparing Eq.(4) and Eq.(6), Λ in Eq.(4) is related to $\langle nn \rangle / \langle \Delta X \Delta X \rangle$. Thus, λ_j represents the ratio of mean square of detector noise to the expected mean square deviation in the change of parameters (structural noise).

The key point is that since W is only reference-related, and does not relate to the position and optical parameters of hidden objects, the inverse matrix $[W^T W + \Lambda]^{-1}$ of a given pattern of the reference system, which can be either homogeneous or inhomogeneous, can be pre-calculated and pre-stored as a database for various patients for clinical use.

Our tests show that this novel inverse procedure converges after only 2–4 iterations, which is much faster than the ART or SART procedures currently used. It takes about one minute to form an image in our reconstruction tests on a Silicon Graphic Instruments (SGI) workstation computer.

To demonstrate the present technique, the following experiment was performed. Schematic drawings of the experimental arrangement are shown in FIGS. 1(a) and 1(b). Ultrashort pulses of 100 fs pulse duration at a wavelength of 625 nm were coupled into a rectangular shape random medium by an optical fiber. This geometry was chosen because it is easy to construct an analytical expression of Green’s function G^0 in a finite sized 3D volume, which is suitable for testing the physical modeling and the inversion algorithm. The scattered pulses around the medium were collected by 7 optical fibers and time resolved by a streak camera. The size of the sample was 60x60 mm and the height was 90 mm. The fibers were located at mid-plane. The source fiber was at the center of the boundary wall. Two fibers each were placed on the opposite and the side boundary walls of the sample, and one fiber detector was placed on the incident wall. The scattered pulses collected by the 7 detection fibers and a reference pulse were coupled onto the input slit of the streak camera for multi-channel detection. The medium was Intralipid solution with a transport mean free path of 2.5 mm and absorption length of about 500 mm. The hidden object was a black painted aluminum rod of diameter of 4.8 mm. Temporal profiles of the scattered pulses around the medium were measured. In this experimental setting, the structure was z-independent, so the reconstructed image is presented as a 2-D image. However, the present method could also be used as a 3-D imaging model.

As an example, a typical set of temporal profiles measured for one S-D pair is shown in FIG. 2. In this case, the detector is located straight across the medium in the line of incidence. Measurements of the uniform medium without the object and with the object placed in three locations 90 degrees apart are also shown. It is clearly shown that the intensity is reduced by introducing the absorbing object, and a larger reduction was observed when the object was placed in the line of the source detector pair. The measurement of 3 object positions is equivalent to 3 measurements by rotating the S-D pairs by 90 degrees while fixing the object location.

In the image reconstruction, an area in the sample was divided into $28 \times 28 = 784$ voxels, which corresponds to an actual voxel size of 2×2 mm. Measurements of 7 S-D pairs with the above mentioned object locations were used. For each temporal intensity profile, intensity data at 40 time slices uniformly distributed from 602 ps to 2045 ps were used. Thus, the total number of input data points was $21 \times 40 = 840$. This is one of the important features of our method—the use of hundreds of time slices from the temporal profile of one S-D pair for image reconstruction gives much more information than data obtained in the frequency domain with much higher speed resolution in sub-mm to mm range to detect a defect. The robustness of the method was demonstrated with a small number of fibers. In our programs, Y and W are magnified by a factor of 100.

Our regularization parameters are spacing independent:

$$\Lambda(r_j) = \lambda_0 \exp(-d\lambda |r_j - r_{center}|) \quad (7)$$

FIGS. 3(a) through 3(e) show images obtained for $X^{(1)}$ in Eq.(4) with different regularization parameters. Using large λ_0 , the image of the hidden object has already appeared after the first iteration. With a decreasing of λ_0 down to 10^{-2} , the image is gradually broken.

FIGS. 4(a) through 4(h) show the results of different numbers of iterations, when the small regularization λ_0 is used. We see that after $m=50$ iterations, the image of the hidden object begins to appear. After $m=500$, the image becomes stable as no visible change in the shape of the object occurs between $m=500$ to $m=2000$.

FIGS. 5(a) and 5(b) show an image obtained where (a) $\lambda_0=1000$, without iteration, by running 1 minute on a Silicon Graphic Incorp. (SGI) Indy computer where $[W^T W + \Lambda]^{-1}$ is stored; and (b) $\lambda_0=10^{-2}$, with 2000 iterations, by running 3 hours on the same computer, respectively. As can be seen, the two images are similar, but the latter has better resolution. Noting that the difference of regularization parameters for these two images is up to 5 orders of magnitude, the stability of the imaging process for the present technique is confirmed.

In both FIGS. 5(a) and 5(b), the presence of an absorber can be clearly seen. The location of the maximum change is about 7 mm away from the center which is about the actual location of the object (10 mm). The full width of half maximum of the absorber is 8 mm which is comparable to the diameter of the object (4.8 mm). The fluctuation at other spatial locations are less than one third of the peak value. Using different regularization parameters, the same location of the absorber was found, but the maximum peak value and the full width of half maximum were different. One possible reason that the center of the image deviates from that of the experimental set is that the hidden object is not a pure transparent scattering absorber, and the possible effect of reflection on the surface of the rod was not included in our physical model.

For comparison, the result using the SART inversion algorithm, commonly used by others, after 100 iterations (taking $X=0$ as initial input), which runs 3 hours on the same SGI workstation, is shown in FIG. 6. There is no clear image of the absorber, noticing that the maximum absorption coefficient is only 0.0025 which is about 40 times smaller than that obtained by our new algorithm.

We have also tested our technique on simulated temporal data with 15% white noise added. A clear image of a single absorber on the correct position was obtained. These results show that our approach is noise-resistant. This inversion method can include a change of diffusion coefficients, $\Delta D(\vec{r})$ or $\Delta u_s(\vec{r})$, as described before for detecting scattering defects in a highly scattering host medium.

It should be noted that a reconstruction algorithm which is suitable for clinical applications must be reasonably rapid in running time while maintaining mathematical integrity. An inverse algorithm mainly based on Fourier transform runs in the fastest way. In order to make a Fourier transform deconvolution available, the condition of "translation invariance" should be satisfied. In other words, the propagator $K(y,x)$ must be the function of $y-x$. This condition is violated in experimental settings in the following three ways: (1) the media is not uniform; (2) there are boundaries on which the light sources and detectors are setting; (3) the propagator here is a function of (r_s, r_d, r) ; therefore, it is impossible to make a Fourier transform for both r_s-r and r_d-r . Among above listed violations, (1) is relatively soft, since we can assume a reference with uniform background, and put non-uniform as an image. On the other hand, reconstruction based on the inverse matrix method does not require the

condition of translation invariance and can be used for more general cases. For purposes of clinical applications, a three-dimensional (3D) reconstruction algorithm is necessary. Because light diffuses in 3D space, the measurements on a specific layer are affected by the hidden objects on other layers. In extending our approach to the 3D case, we face a new difficulty. The computational complexity to inverse a matrix is about N^3 , where N is the size of the matrix. If one supposes that the size on the third dimension is divided into 30 grids, the computing complexity to inverse a matrix in the 3D case is about 27,000 times that in the 2D case, which makes the precomputation of an inverse matrix for 3D case unfeasible. To overcome this difficulty, we propose adding a 1D Fourier transform to the 2D matrix inversion.

Therefore, a novel inverse algorithm for obtaining images of 3D objects hidden in scattering media is taught in this invention, the method combining a 2D matrix inversion with a 1D Fourier transform inversion. In our approach the conditions for Fourier transform available are properly treated. This method greatly reduces the computational burden, compared to standard 3D matrix inversion methods. This approach can be used for both time-resolved data and frequency domain data. Using the above mentioned pre-computation and database storage strategy, we tested the present technique. It takes about 30 minutes on a Silicon Graphic Indy 4400 computer to obtain a 3D image of $28 \times 28 \times 32$ voxels of mm objects in cm's scattering media.

The source-detector pairs are arranged on the boundary of scattering media, such as breast and brain, in a 2D plane (the x-y plane), which is scanned along the z direction. Accordingly, z coordinates of sources and detectors are the same, thereby eliminating the violation (3) mentioned above. The reference system is assumed to be uniform and infinite along the z direction. This assumption leads to some deviation in the reconstructed image due to finite z-size in experimental setting. Since there is no source and detector setting on the z-end plane, this end effect becomes less serious. Under the above experimental setting and assumption, W satisfies z-translation invariance. In other words, it is a function of $z-z_0$, where z_0 is z-position of source-detector plane and z is z-coordinate of a voxel. After making a one-dimensional Fourier transform over $z-z_0$ we obtain K independent 2D matrices, $W_{2D}(k)$, parameterized by k , with K the number of grid-points in the Fourier k-space. We separately calculate the K inverse matrices $[W_{2D}(k)^T W_{2D}(k) + \Lambda(k)]^{-1}$, $k=1, 2, \dots, K$, where $\Lambda(k)$ is a matrix for regularization. These inverse matrices are stored as database for later reconstruction of image in different hidden object cases. The computational complexity now is K times that of inverse of a W_{2D} matrix, which is much less than that of inverse of a W_{3D} matrix.

The experimental data in time-resolved (or frequency domain) are $Y(r_d, r_s, t(\omega), z_0)$, where r_d and r_s are (x,y) coordinates of detector and source, respectively, and t is the slice (or ω is frequency). We make a Fourier transform over z_0 to obtain $Y(r_d, r_s, t(\omega), k)$, $k=1, 2, 3, \dots, K$. We then obtain the image in the k space using the following matrix multiplication:

$$X(k) = Y(k)^T W_{2D}(k) [W_{2D}(k)^T W_{2D}(k) + \Lambda(k)]^{-1}, \quad k=1, 2, 3, \dots, K$$

Then, the inverse 1D Fourier transform of $X(k)$ over k generates the 3D distribution of the change of absorption coefficients or scattering coefficients.

A simulated experimental setting for a 3D image obtained using a plurality of source-detector (S-D) pairs is shown in FIGS. 7(a) and 7(b). The S-D pairs are arranged around a square of size $60 \times 60 \text{ mm}^2$. This arrangement of S-D pairs is

then rotated 90 degrees and 180 degrees and the plane is scanned 32 steps along z in a range of 120 mm. For each simulated temporal profile, intensities at 40 time slices uniformly distributed from 602 ps to 2045 ps are taken. The number of sampling data are $7 \times 3 \times 40 \times 32$. Data both with and without hidden objects are computed to produce $Y = -100 \ln(I/I_0)$, adding uniform distributed noise in $\pm 10\%$ range, where I and I_0 are intensity with and without hidden objects, respectively. The volume of sample is divided into $28 \times 28 \times 32$ voxels. Two arrangements of hidden absorption objects are separately shown in FIGS. 8(a) and 8(b). The cross-sections of the hidden objects are $4 \times 4 \text{ mm}^2$ and $6 \times 6 \text{ mm}^2$. In case (a), both objects are located from the 9th z -layer to the 13th z -layer (about 20 mm in length). In case (b), one is located from the 9th layer to the 13th layer (about 20 mm in length) and another is located from 17th layer to the 20th layer (about 16 mm in length). The W is calculated using Green's function method based on the diffusion equation. For absorbing coefficients, it is given by the following equation:

$$W_{3D}(r_s, r_d, r, z - z_0, t) = \frac{(4\pi Dc\tau)^{1/2}}{G_{2D}^0(r_s, r_d, t)} \int_0^r d\tau G_{2D}^0(r_d, r, t - \tau) G_{2D}^0(r, r_s, \tau) \times [4\pi Dc(t - \tau)]^{-1/2} [4\pi Dc\tau]^{-1/2} \exp\left(-\frac{t(z - z_0)^2}{4Dc(t - \tau)\tau}\right)$$

Where G_{2D}^0 is 2D Green's function for reference, D is the diffusion constant and c is the speed of light in the medium. Scattering objects with different l_s can be also calculated as mentioned above for 2D case. The background transport mean free path is chosen as $l_s^0 = 2.5 \text{ mm}$, and the absorption length $l_a^0 = 500 \text{ mm}$. The absorbing objects have $l_a = 2.5 \text{ mm}$. In making Fourier transform and computing inverse matrix $[W_{2D}(k)^T W_{2D}(k) + \Lambda(k)]^{-1}$, the regularization matrix is set as $\Lambda(k) = (\lambda + \beta k^2)I$, with λ and β are parameters for regularization. In this calculation $\lambda = 10^2$ and $\beta = 0$ are taken. The images of the absorption objects are separately shown in FIG. 9(a) and FIG. 9(b), which correspond to FIGS. 8(a) and FIG. 8(b), respectively. In FIGS. 9(a) and 9(b), index K is the index of layer in z coordinate. The images of hidden objects appear in the right layers where the objects are arranged, with a resolution of about 4 mm. There are some aliased images appearing near the z -end because of discrete sampling.

The experimental arrangement for implementing the present technique when using electronic time-gated imaging camera (TGIC) system is shown schematically in FIGS. 10(a) and 10(b). Ultrashort light pulses of approximately 100 fs duration from a Ti:sapphire laser and amplifier system operating at a wavelength of 800 nm and a repetition rate of 1 kHz are launched into the scattering medium in which the object is embedded. One preferred shape of the random medium is a cylindrical disc. The radius of the disc is preferably much larger than its thickness. The cylindrical geometry is chosen because it is easier to construct an analytical expression for Green's function for testing the physical model and inversion algorithm.

The emergent pulse from the other end face of the cylindrical sample holder is amplified and different temporal slices of the pulse are recorded by the electronic time-gated image intensifier and CCD camera system. The output of the TGIC system is a shadowgram-like image, or more generally, a two-dimensional time-dependent intensity distribution $I(x, y, t)$. These are shown schematically in FIG.

10(b) as sequence of frames. Integrated intensity over the same small area of all the shadow images in the sequence plotted as a function of gate position generates a temporal intensity profile, also displayed in FIG. 10(b) above the sequence of image frames. Temporal intensity profiles may also be obtained by plotting the average intensity over a small area or the intensity value at a particular point on the shadow images as a function of gate position. $I(x, y, t)$ may be readily converted to $Y(\rho_{ds}, \phi_{ds}, t)$ for use in the inversion algorithm.

The sample we used was a glass slide on which scattering particles of size varying from 0.1–1.5 mm were attached. It was placed at the center of the 5.5 cm thick sample cell. The scattering medium was a 1% solution of Intralipid 10% in water. A sequence of four frames taken at gate positions of $-50, 0, +50$ and $+100$ ps are displayed in FIG. 11 as frames (a), (b), (c) and (d), respectively. The zero time corresponds to the arrival time of the ballistic light that is determined by performing the experiment using clear water in the sample cell. The sequence of frames clearly demonstrates that at later times the diffusive photons blur out the shadow image, as in frame (d). For highly-scattering thick samples, such as human breast, blurred images as in frame (d) or worse are expected. The present invention provides an algorithm to reconstruct images from such blurred shadows. The sequence of temporal slices, that is, the shadowgrams taken at different time intervals enables determination of location of the object inside the scattering medium.

Scattering light pulse from the side wall of the cylindrical cell may be collected as well, as shown in FIG. 10(b), to provide additional intensity profiles for image reconstruction. Scattered light pulse from the side wall may be recorded using the same camera system, or preferably another identical camera system or systems. Sample cells of other geometries, such as a cube, a rectangular parallelepiped, or of an arbitrary shape may also be used with corresponding modifications of image reconstruction algorithm.

The following comments, observations, objects, features, uses, applications and/or advantages may be made about the present invention:

- (1) Temporal intensities extracted at multiple time slices of scattered light profile measured using multiple source detector pairs around turbid media are used as input data for the inversion to obtain the image maps of the media.
- (2) An image reconstruction algorithm for imaging highly scattering turbid media is developed. The inversion procedure consists of input scattered light intensity data at different time slices, physical modeling of light propagation in random media, inversion computation algorithm, reconstructed image of spatial distributions of key optical parameters of random media, and image displays.
- (3) Using different theoretical models for describing photon migration in random media for imaging. The theory includes transport theory for photon migration, and its approximations, such as the diffusion theory and the telegraph equations.
- (4) Key optical parameters, such as the absorption coefficient, the index of refraction, the transport scattering length, the scattering length, and the diffusion constant, are mapped for imaging the internal structure of the turbid media at different light wavelengths. A difference in both absorption and scattering can be imaged to form a map of the internal structure of the turbid media in 3-D.

- (5) A fast inversion algorithm is developed based on Shaw's principle, Eq. (4), in which the weight function matrix, W (Eq.(3)), which relates a change in the properties of turbid media to the changes in measured light intensities, can be pre-computed and stored for fast image inversion for each patient.
- (6) A cumulant formula is developed to relate the experimentally measured intensities to the prediction from theoretical models based on properties of the turbid media.
- (7) 3-D images of spatial distribution of key optical parameters of turbid media can be obtained using this algorithm. 2-D slices of tomographic images can be obtained by taking a section of a 3-D image and displaying it to highlight the location of tumors.
- (8) Use the algorithm to image non-invasively tumors and abnormality in human body, such as tumor growths in breasts, tumors in brain, cerebral hemorrhage in brain, hemorrhage in internal organs, prostate.
- (9) Using the algorithm with temporal data at various NIR wavelengths from 700 to 1500 nm for image reconstruction for monitoring metabolic states of a given part of human body in vivo.
- (10) This novel inverse reconstruction method can be combined with shadowgram type of image techniques to further improve spatial resolution and enhance the presence of the abnormality.
- (11) Use single source optical fiber and multiple detector fibers for collecting temporal profiles of the scattered pulses.
- (12) Use multiple input source fibers and multiple detector fibers for collecting temporal profiles of the scattered pulses. A time sharing beam deflector will be incorporated to switch the input from one source fiber to another.
- (13) Multiple S-D optical fibers are mounted on bra-like or hat-like holders surrounding a breast or a head (brain) to detect temporal intensity profiles of scattered pulses from breast or head (brain) for imaging the internal structure of optical properties.
- (14) The lasers used for imaging are Cr^{4+} Forsterite, Cr^{4+} YAG, semiconductor lasers, Nd:YAG, and/or Ti:Sapphire lasers. The laser pulses at different wavelengths will be coupled to optical fiber by a time sharing scheme to deliver to the scattering media for spectral imaging.
- (15) Temporal intensity profiles of scattered pulses around scattering media are measured using time resolved detection methods, including streak camera, ultrafast pin diodes, fast photomultipliers.
- (16) Time-resolved shadowgram-type images and their intensity profiles obtained using the electronic time-gated image intensifier and CCD camera system will provide a plurality of profiles. For example, the TGIC system we presently use includes a 384×284 pixel CCD camera. Each pixel in this arrangement may be looked upon as a detector fiber in the one-source-7-detector arrangement that has been described above. Thus, the data collection time is shortened and the use of a plurality of profiles increase the spatial resolution of reconstructed image. Since the shadow images are taken sequentially in time the depth information and hence the location of the object inside the medium is obtained.
- (17) Reconstructed images are to be displayed in 3-D or in 2-D tomography slices.

- (18) Manipulating images obtained from claim 9 at different wavelengths to construct difference, sum, ratio and/or sum of ratio image maps at two wavelengths or several wavelengths to highlight tumors and to differentiate benign from malignant tumors.

The embodiments of the present invention described above are intended to be merely exemplary and those skilled in the art shall be able to make numerous variations and modifications to it without departing from the spirit of the present invention. All such variations and modifications are intended to be within the scope of the present invention as defined in the appended claims.

What is claimed is:

1. A method of imaging an object located in a highly scattering turbid medium, the high scattering turbid medium being an in vivo biological tissue, said method comprising the steps of:

- illuminating the object through the highly scattering turbid medium with a pulse of light, the light emergent from the highly scattering turbid medium consisting of a ballistic component, a snake-like component and a diffusive component;
- determining the intensity of said diffusive component at a plurality of points in time; and
- using said intensity determinations to form an image of the object in the highly scattering turbid medium, said using step comprising using a mathematical inversion algorithm to generate an image of the highly scattering turbid medium, said mathematical algorithm being

$$X^{(k+1)T} = [Y^T W + X^{(k)T} \Lambda] [W^T W + \Lambda]^{-1}$$

wherein W is a matrix relating output at source and detector positions r_s and r_d , respectively, at time t to position r , Λ is a regulation matrix, chosen for convenience to be diagonal but selected in a way related to the ratio of the noise, $\langle nn \rangle$ to fluctuations in the absorption (or diffusion) X_j that we are trying to determine:

$$\Lambda_{ij} = \lambda_j \delta_{ij} \text{ with } \lambda_j = \langle nn \rangle / \langle \Delta X_j \Delta X_j \rangle$$

Y is the data collected at the detectors, and X^k is the k th iterate toward the desired absorption information.

2. The method as claimed in claim 1 wherein said pulse of light has a wavelength in the visible to near infrared region of the spectrum.

3. The method as claimed in claim 2 wherein said pulse of light has a wavelength of about 700 nm to about 1500 nm.

4. The method as claimed in claim 1 wherein said pulse of light is an ultrashort pulse of light.

5. The method as claimed in claim 1 wherein said pulse of light is a laser pulse emitted from a laser selected from the group consisting of Ti:Sapphire lasers, Cr^{4+} Forsterite lasers, Cr^{4+} YAG lasers, semiconductor lasers and Nd:YAG lasers.

6. The method as claimed in claim 1 wherein said in vivo biological tissue is selected from the group consisting of in vivo human breast tissue, in vivo human brain tissue, in vivo human neck tissue and in vivo human prostate tissue and wherein said object is a tumor.

7. The method as claimed in claim 1 further comprising the step of detecting cancerous tumors in said in vivo biological tissue using fluorescence spectroscopy.

8. The method as claimed in claim 1 wherein said determining step comprises measuring the intensity of light

at a plurality of points in the time frame spanning from 50 ps to 10 ns after illumination.

9. The method as claimed in claim 8 wherein said determining step comprises measuring the intensity of light at hundreds of points in the time frame spanning from 50 ps to 10 ns after illumination.

10. The method as claimed in claim 9 wherein said hundreds of points are determined by slicing the time frame into equal portions.

11. A method of forming a map of a highly scattering turbid medium, the high scattering turbid medium being an in vivo biological tissue, said method comprising the steps of:

- (a) illuminating the highly scattering turbid medium with a first pulse of light along a first axis of incidence, whereby the light emergent from the highly scattering turbid medium due to said first pulse of light consists of a ballistic component, a snake component and a diffusive component;
- (b) determining, at a plurality of times, the intensity of said diffusive component of the first pulse of light emergent from the highly scattering turbid medium at a plurality of locations;
- (c) illuminating the highly scattering turbid medium with a second pulse of light along a second axis of incidence, said second axis of incidence intersecting with said first axis of incidence, whereby the light emergent from the highly scattering turbid medium due to said second pulse of light consists of ballistic component, a snake component and a diffusive component;
- (d) determining, at a plurality of times, the intensity of said diffusive component of the second pulse of light emergent from the highly scattering turbid medium at a plurality of locations; and
- (e) using the intensity determinations from steps (b) and (d) to generate a map of the highly scattering turbid medium, said using step comprising using a mathematical inversion algorithm to generate said map, said mathematical algorithm being

$$X^{(k+1)T} = [Y^T W + X^{(k)T} \Lambda] [W^T W + \Lambda]^{-1}$$

wherein W is a matrix relating output at source and detector positions r_s and r_d , respectively, at time t to position r, Λ is a regulation matrix, chosen for convenience to be diagonal but selected in a way related to the ratio of the noise, $\langle nn \rangle$ to fluctuations in the absorption (or diffusion) X_j that we are trying to determine:

$$\Lambda_{ij} = \lambda_j \delta_{ij} \text{ with } \lambda_j = \langle nn \rangle / \langle \Delta X_j \Delta X_j \rangle$$

Y is the data collected at the detectors, and X^k is the kth iterate toward the desired absorption information.

12. The method as claimed in claim 11 wherein each of said first and said second pulses of light has a wavelength in the visible to near infrared region of the spectrum.

13. The method as claimed in claim 11 wherein each of said first and said second pulses of light has a wavelength of about 700 nm to about 1500 nm.

14. The method as claimed in claim 11 wherein each of said first and said second pulses of light is an ultrashort pulse of light.

15. The method as claimed in claim 11 wherein each of said first and said second pulses of light is a laser pulse

emitted from a laser selected from the group consisting of Ti:Sapphire lasers, Cr^{4+} Forsterite lasers, Cr^{4+} YAG lasers, semiconductor lasers and Nd:YAG lasers.

16. The method as claimed in claim 11 wherein said in vivo biological tissue is selected from the group consisting of in vivo human breast tissue, in vivo human brain tissue, in vivo human neck tissue and in vivo human prostate tissue and wherein said object is a tumor.

17. The method as claimed in claim 11 wherein said determining steps each comprise time-resolving light emergent from the highly scattering turbid medium.

18. The method as claimed in claim 11 further comprising the steps of:

- (f) illuminating the highly scattering turbid medium with a third pulse of light along a third axis of incidence, said third axis of incidence intersecting a plane defined by said first and second axes of incidence, whereby the light emergent from the highly scattering turbid medium due to said third pulse consists of a ballistic component, a snake component and a diffusive component; and
- (g) determining, at a plurality of times, the intensity of said diffusive component of the third pulse of light emergent from the highly scattering turbid medium at a plurality of locations;
- (h) wherein said using step comprises using the intensity determinations from steps (b), (d) and (g) to generate a map of the highly scattering turbid medium.

19. The method as claimed in claim 11 further comprising the step of detecting cancerous tumors in said in vivo biological tissue using fluorescence spectroscopy.

20. The method as claimed in claim 11 wherein said determining step comprises measuring the intensity of light at a plurality of points in the time frame spanning from 50 ps to 10 ns after illumination.

21. The method as claimed in claim 11 wherein said determining step comprises measuring the intensity of light at hundreds of points in the time frame spanning from 50 ps to 10 ns after illumination.

22. The method as claimed in claim 21 wherein said hundreds of points are determined by slicing the time frame at regular intervals.

23. The method as claimed in claim 11 wherein said map is an absorption map.

24. The method as claimed in claim 11 wherein said map is a scattering map.

25. An apparatus for imaging an object located in a highly scattering turbid medium, said apparatus comprising:

- (a) means for illuminating the object through the highly scattering turbid medium with a pulse of light, the light emergent from the highly scattering turbid medium consisting of a ballistic component, a snake-like component and a diffusive component;
- (b) means for determining the intensity of said diffusive component at a plurality of points in time; and
- (c) means for using said intensity determinations to form an image of the object in the highly scattering turbid medium, said using means comprising a computer programmed to perform a mathematical inversion algorithm, said mathematical algorithm being

$$X^{(k+1)T} = [Y^T W + X^{(k)T} \Lambda] [W^T W + \Lambda]^{-1}$$

wherein W is a matrix relating output at source and detector positions r_s and r_d , respectively, at time t to

position r , Λ is a regulation matrix, chosen for convenience to be diagonal but selected in a way related to the ratio of the noise, $\langle nn \rangle$ to fluctuations in the absorption (or diffusion) X_j that we are trying to determine:

$$\Lambda_{ij} = \lambda_j \delta_{ij} \text{ with } \lambda_j = \langle nn \rangle / \langle \Delta X_j \Delta X_j \rangle$$

Y is the data collected at the detectors, and X^k is the kth iterate toward the desired absorption information.

26. The apparatus as claimed in claim 25 wherein said illuminating means comprises a plurality of light sources and wherein said determining means comprises a plurality of light detectors.

27. The apparatus as claimed in claim 26 wherein 7 to 50 light source/light detector combinations are used to generate a 2 to 10 mm map of a breast tissue 5 to 10 cm thick.

28. A method of forming a map of a highly scattering turbid medium, said method comprising the steps of:

- (a) illuminating the highly scattering turbid medium with a first pulse of light along a first axis of incidence, whereby the light emergent from the highly scattering turbid medium due to said first pulse of light consists of a ballistic component, a snake component and a diffusive component;
- (b) determining, at a plurality of times, the intensity of said diffusive component of the first pulse of light emergent from the highly scattering turbid medium at a plurality of locations;
- (c) illuminating the highly scattering turbid medium with a second pulse of light along a second axis of incidence, said second axis of incidence intersecting with said first axis of incidence, whereby the light emergent from the highly scattering turbid medium due to said second pulse of light consists of ballistic component, a snake component and a diffusive component;
- (d) determining, at a plurality of times, the intensity of said diffusive component of the second pulse of light emergent from the highly scattering turbid medium at a plurality of locations; and
- (e) using the intensity determinations from steps (b) and (d) to generate a map of the highly scattering turbid medium, said using step comprising using a mathematical inversion algorithm to generate said map, said mathematical inversion algorithm combining a two-dimensional matrix inversion with a one-dimensional Fourier transform inversion.

29. The method as claimed in claim 28 wherein said first and second pulses of light are emitted from respective sources, wherein said determining step is performed with detectors located at said plurality of locations, said source and detectors being arranged in a 2D plane (the x-y plane), which is scanned along the z direction, the reference system being assumed to be uniform and infinite along the z direction and wherein, under above experimental setting and assumption, satisfies translation invariance in z coordinate and is a function of $z-z_0$, where z_0 and z are the z-positions of said 2D plane, and of a voxel, respectively.

30. The method as claimed in claim 28 further comprising the steps of:

- (a) making a one-dimensional Fourier transform over $z-z_0$ to obtain K independent 2D matrices, $W_{2D}(k)$, parameterized by k , with K the number of grid-points in the Fourier k-space;
- (b) calculating the inverse matrices $[W_{2D}(k)^T W_{2D}(k) + \Lambda(k)]^{-1}$, $k=1,2,3, \dots, K$, where $\Lambda(k)$ is a matrix for

regularization, said inverse matrices being stored as a database for later reconstruction of image in different hidden object cases;

- (c) obtaining experimental data in time-resolved domain (or in frequency domain), $Y(r_d, r_s, t(\omega), z_0)$, where r_d and r_s are (x,y) coordinates of detector and source, t is time slice (or ω is frequency), and making a Fourier transform over z_0 to obtain $Y(r_d, r_s, t(\omega), k)$, $k=1,2,3, \dots, K$;
- (d) using the following matrix multiplication to obtain K images in Fourier k-space:

$$X(k) = Y(k)^T W_{2D}(k) [W_{2D}(k)^T W_{2D}(k) + \Lambda(k)]^{-1}, \quad k=1,2,3, \dots, K; \text{ and}$$

- (e) making an inverse 1D Fourier transform of $X(k)$ over k to obtain the 3D distribution of the change of absorption coefficients or scattering coefficients.

31. The method as claimed in claim 30 wherein a multi-CPU computer is used to compute in parallel K components of $X(k)$ in step (d) of claim 30.

32. The method as claimed in claim 28 wherein said mathematical inverse algorithm is used for time-resolved data and frequency domain data.

33. The method as claimed in claim 28 wherein said 3D image of both scattering coefficients and absorption coefficients of hidden objects is obtained through said mathematical inverse algorithm.

34. The method as claimed in claim 28 wherein said 3D image of scattering coefficients of hidden scattered objects in scattering media of different scattering length is obtained through said mathematical inverse algorithm.

35. The method as claimed in claim 29 wherein the shape of the highly scattering medium is cylindrical, or rectangular or that with other shape of (x-y) cross section.

36. The method as claimed in claim 29 wherein the scanning steps in z direction are 16 to 128 to generate an image with 16 to 128 layers in z direction.

37. The method as claimed in claim 29 wherein the sources and detectors are fixed on different layers and wherein a computer-control switch is used to shine the sources sequentially.

38. The method as claimed in claim 29 wherein the sources and detectors are located on the boundary of the highly scattering turbid medium or inside the highly scattering turbid medium.

39. The method as claimed in claim 29 wherein the highly scattering turbid medium is an in vivo biological organ selected from the group consisting of human breast, human brain, human neck, human prostate, heart, limb, cervix and kidney.

40. The method as claimed in claim 1 wherein the detector is an area camera, such as a CCD, and equipped with means to record temporal slices of the scattered pulse, such as, a gated image intensifier.

41. The method as claimed in claim 40 wherein the gated image intensifier has a gate width of 80 ps and gate position can be changed in steps of 25 ps.

42. The method as claimed in claim 40 wherein the in vivo biological tissue is from a human breast, said in vivo biological tissue being disposed in a cell sample holder, and wherein said cell sample holder contains in addition to the in vivo biological tissue an index-matched fluid of similar scattering characteristics.

43. The method as claimed in claim 42 wherein the cell sample holder is cylindrical.

44. The method as claimed 42 wherein the cell sample holder has a cube-like, sphere-like or any other geometrical shape.

21

45. The method as claimed in claim **40** wherein the in vivo biological tissue is disposed in a cell sample holder and wherein the scattered light is collected from end faces and/or side faces of the cell sample holder.

46. The method as claimed in claim **45** wherein the gated image intensifier has a gate width of 80 ps and gate position can be changed in steps of 25 ps.

47. The method as claimed in claim **45** wherein a time sequence of images frames is taken with a 80 ps gate and frames are taken in steps of 25 ps from -5 ns to +15 ns, and used for image reconstruction employing said mathematical inversion algorithm.

48. The method as claimed in claim **47** wherein a suitable gate width between 5 ps to 1 ns and a sequence of time

22

frames from -5 to +15 ns are taken, and used for image reconstruction employing said mathematical inversion algorithm.

49. The method as claimed in claim **45** wherein said mathematical inversion algorithm is modified in accordance with the geometry of the cell sample holder.

50. The method as claimed in claim **45** wherein the time sequences of image frames are taken at angles from 0 to 90 degrees with respect to the optical axis and used for image reconstruction employing the mathematical inversion algorithm.

51. The method as claimed in claim **47** further comprising the step of detecting tumors in vivo inside human body using fluorescence spectroscopy.

* * * * *